Accepted Manuscript

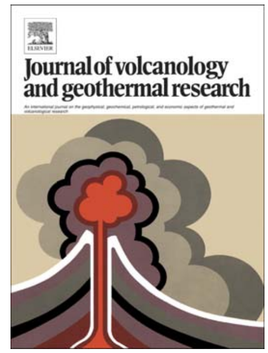

Geology of the Vilama caldera: a new interpretation of a large-scale explosive event in the Central Andean plateau during the Upper Miocene

M.M. Soler, P.J Caffe, B.L. Coira, A.T. Onoe, S. Mahlburg Kay

PII: S0377-0273(07)00084-4
DOI: doi: 10.1016/j.jvolgeores.2007.04.002
Reference: VOLGEO 3668

To appear in: *Journal of Volcanology and Geothermal Research*

Received date: 27 April 2006
Revised date: 14 November 2006
Accepted date: 11 April 2007

Please cite this article as: Soler, M.M., Caffe, P.J., Coira, B.L., Onoe, A.T., Kay, S. Mahlburg, Geology of the Vilama caldera: a new interpretation of a large-scale explosive event in the Central Andean plateau during the Upper Miocene, *Journal of Volcanology and Geothermal Research* (2007), doi: 10.1016/j.jvolgeores.2007.04.002

Geology of the Vilama caldera: a new interpretation of a large-scale explosive event in the Central Andean plateau during the Upper Miocene.

M.M. Soler[a], P.J Caffe[a,*] , B.L. Coira[a], A.T. Onoe[b], S. Mahlburg Kay[c]

[a]- CONICET and Instituto de Geología y Minería. Universidad Nacional de Jujuy. Av. Bolivia 1661. San Salvador de Jujuy (CP 4600). Jujuy. Argentina.

[b]- Centro de Pesquisas Geocronológicas (CPGeo) – Instituto de Geociências – Universidade de São Paulo. Rua do Lago 562, Cidade Universitária. São Paulo. CEP 05508-900. Brasil.

[c]- Cornell University, Department of Earth and Atmospheric Sciences, 3140 Snee Hall, Ithaca, NY 14853, U.S.A

[*] Corresponding author
email: pabcaffe@idgym.unju.edu.ar
tel: + 54 388 4221593
fax: + 54 388 4232957

Abstract

The Vilama caldera is one of the very large-volume volcanic structures that formed during the ignimbrite flare-up that lasted from 10 Ma to 4 Ma on the central Andean plateau. Formerly, the Vilama structure was interpreted as a 65 x 40 km wide caldera with a two stage evolution. New field correlations, petrographical, geochemical and geochronological data lead to a substantially larger reinterpreted Vilama ignimbrite, whose outcrops cover more than 4000 km^2. New and existing K/Ar and Ar/Ar dating shows that the dacitic Vilama ignimbrite erupted from the Vilama caldera at 8.4-8.5 Ma. The ignimbrite can be divided into extracaldera outflow and intracaldera deposits. The outflow has a mean thickness of ~40 m and is separated into a restricted valley-ponded lower cooling unit, and a laterally extensive low aspect ratio upper cooling unit.

The Vilama caldera, which is roughly rectangular (35-40 km x 15-18 km) in shape and has central coordinates of 22°24'S and 66°57'W, is considered to have formed in a single-stage collapse event. As the topographic rim is only seen on the western side, the extent of collapse and geometry of the caldera are incompletely known and inferred from indirect data. Possible collapse geometries include a slightly asymmetric single-block subsidence and non-chaotic multiple-block collapse. Estimated erupted volumes range from ~1800 to 1200 km^3, or 1400 to 1000 km^3 in dense rock equivalents.

The properties of the Vilama ignimbrite which include a crystal-rich and pumice-poor nature, a high degree of welding and induration and a prodigious volume, suggest that an external drive, rather than volatile overpressures controlled and maintained the eruption. The best candidate is caldera subsidence triggered by the instability of a magma chamber roof above a batholith-scale magma body. Transtensive/distensive tectonic stresses resulted in the northwest elongation of the magma chamber and influenced the roughly rectangular/subelliptical shape of the subsided block.

As most of the Vilama ignimbrite is within the caldera, subsidence must have started early in the eruptive history. Immediately before, or concomitantly with the onset of subsidence, the lower extracaldera unit was deposited from flows that formed during collapse of well-developed plumes with efficient convective phases. Once caldera collapse was completely established, the eruption dynamic changed dramatically, and the extracaldera and intracaldera facies erupted. During this phase, unstable and low plumes (boiling-over collapse fountains) preferentially collapsed towards the interior of the subsiding structure, causing the ignimbrite volume to be concentrated in the caldera. After much less than 1 Ma, resurgence, which might be linked to magma chamber recharge, domed the intracaldera facies and caused post-collapse volcanism to be channeled through subsidence and/or resurgence-related faults.

Keywords: Vilama caldera; Central Andes; APVC region; caldera collapse; large-volume ignimbrites.

1. Introduction

The Central Andean volcanic zone (14°-28° S) comprises the main active volcanic arc, and a broad back-arc belt (50-150 km wide) located to the east, which is composed of the eruptive products of calderas, stratovolcanoes and monogenetic centers of Oligocene to Pleistocene age. This region includes the Altiplano-Puna plateau, an area which, from the upper Miocene to Pleistocene, hosted several large-volume explosive eruptions which resulted in the deposition of extensive ignimbrites of predominantly dacitic composition (*ignimbrite flare-up*; de Silva, 1989a; Coira et al., 1993; Kay et al. 1999). Particularly, the central portion (21° - 24°S) of the plateau exhibits a conspicuous concentration of large-volume Neogene ignimbrites. de Silva (1989a) named this enormous (~70000 km^2) silicic volcanic field the

Altiplano Puna Volcanic Complex (APVC; Fig. 1), and postulated that these extensive ignimbrites originated during collapse of several volcanic calderas of large dimensions (10s of km in diameter).

Some of the largest caldera structures in the APVC had been identified by the late 1970s (Francis and Baker, 1978), but a comprehensive characterization of these features has been delayed by problems in correlations of the ignimbrites and their assignment to eruptive sources. One problem has been that the eruptive activity of the various centers has produced a complex stratigraphy, in which similar volcanic units commonly interfinger with, or are almost completely covered by eruptions from broadly contemporaneous centers. Another is that the low degrees of erosion and near lack of tectonic disruption, which have allowed volcanic edifices to be well preserved, have also resulted in a paucity of outcrops showing vertical sections, especially in intracaldera sequences. A third is that general field, petrographic and geochemical similarities (de Silva, 1989b) and small age differences (e.g. Caffe et al., 2006) between the ignimbrites make them difficult to correlate without detailed studies. These problems have been aggravated by the poor access to the region and the high altitude (>4000 masl).

Thus, among the giant structures originally identified as APVC calderas (de Silva, 1989b; de Silva and Francis, 1991) (Fig. 1), only a few have been subjected to detailed volcanological and stratigraphic work [e.g. Panizos (Ort, 1993), Coranzulí (Seggiaro, 1994), and La Pacana (Gardeweg and Ramírez, 1987; Lindsay et al., 2001a)]. The rest have only been subjects of regional mapping or reconnaissance studies.

In this paper we focus on the stratigraphy and eruptive history of one of the largest and least-known collapse calderas of the APVC: the Vilama caldera (Fig. 1). This center was described and mapped (see Fig. 2) in a reconnaissance study by Coira et al. (1996). In the model presented in that paper, the Vilama caldera was seen as comprising two main collapse episodes linked to the eruptions of two extensive pyroclastic deposits (Granada and Vilama ignimbrites, see Fig. 2). Since that time, Caffe et al. (2006) have redefined the eruptive vent location for the Granada ignimbrite, and shown that it is unrelated to the Vilama caldera. The 'two step' eruptive model proposed for the Vilama caldera is in need of substantial revision.

Detailed new field, stratigraphic, petrographic, geochemical and geochronological data are used in this study to redefine the geographical distribution and correlation of the Vilama ignimbrite units and to reinterpret the position and shape of the Vilama caldera. The new model allows the volume of the Vilama ignimbrite to be better constrained, and suggests that the collapse of the Vilama caldera involved one of the largest super explosive volcanic events described on Earth.

2- Previous work on the Vilama caldera and identification of problems

Previously, Coira et al. (1996) envisaged the Vilama caldera as a giant (~65 x 40 km) structure with central coordinates of 22°36'S and 66°51'W (Fig. 2) that erupted in two main stages. The first eruption was considered to be associated with the emplacement of the Granada ignimbrite during a trap-door collapse event. More recent studies by Caffe et al. (2006) have redefined the Granada ignimbrite and shown that is has an areal distribution of ~630 km^2, which is much reduced from the ~ 2300 km^2 estimated by Coira et al. (1996). Caffe et al. (2006) characterize the Granada ignimbrite as a high aspect ratio, compound ignimbrite with an estimated total erupted volume of ~100-120 km^3. The new map pattern and the redefined stratigraphic characteristics show that the Granada ignimbrite was not erupted from a trap-door structure related to the Vilama caldera. Instead, Caffe et al. (2006) propose that the Granada ignimbrite is older, having erupted by ~ 10 Ma, and that the source was a smaller volcanic structure centered at 22°34'S, 66°35'W and subsequently covered by the 9 to 5 Ma volcanic deposits from the Abra Granada volcanic complex (Soler, 2005).

The second collapse of the Vilama caldera described by Coira et al. (1996) was postulated to be linked to the emplacement of the Vilama ignimbrite in a downsag episode (Fig. 2) that used part of the previous trap-door collapse structure. A curious feature of this model was that the intracaldera facies were thought to cover an extensive (>2500 km^2) area and to be thin (<15 m thick, on average), whereas the outflow facies were thought to be thicker (up to 70 m) and more areally restricted (<200 km^2) (Fig. 2). This unusual facies distribution resulted from problems in correlating geologic units on maps across the border between Argentina and Bolivia, and reliance on sparsely distributed stratigraphic, geochemical and geochronological data. The mapping (Fig. 2) resulted in the splitting of the Vilama ignimbrite as redefined here into several units. The revised distribution of the Vilama ignimbrite presented here requires a major reinterpretation of the eruptive style and evolution of the Vilama caldera.

3. Redefinition of the Vilama ignimbrite

3.1. Correlation

The general characteristics of undisputed outcrops of the Vilama ignimbrite, as defined by Coira et al. (1996), have been used in this study as a basis to evaluate and correlate volcanic units in Bolivia and Argentina that could be related to the Vilama eruption. To this end, detailed stratigraphic sections were examined at some 27 different sites (Fig. 3). Some sections had been described previously, others are new sections that were selected for their resemblance to typical Vilama ignimbrite rock units on satellite images or aerial photographs. Detailed descriptions of all sections can be found in Soler (2005).

The typical Vilama ignimbrite as described by Coira et al. (1996) consists of a reddish to pink, moderately to densely welded, crystal-rich ash-flow tuff. The massive character and absence of intercalated plinian fall or surge deposits in the ignimbrite are distinctive features. The Vilama ignimbrite deposits also often show a well-developed subhorizontal jointing, which is usually coincident with foliation planes in the areas of the densest welding. Overall, the Vilama ignimbrite has a modest pumice (fiamme) content, and is very poor in lithic fragments. The pumice and whole rock phenocryst assemblage includes quartz, plagioclase (andesine), partially altered biotite (the predominant Fe-Mg phase), and varying, but always present, ortho- and clinopyroxene, hornblende and opaque minerals. Modal proportions among the different crystalline phases are typically very variable. The K/Ar age of the unit was reported to be ~8.5 Ma (AQUATER, 1979).

Many ignimbrite sections that were not originally included in the Vilama ignimbrite, crop out in Bolivia and Argentina in the vicinity of the typical Vilama units. Some of these sections have characteristics like the typical Vilama units and are readily correlated. Table 1 shows a list of these correlations, provides a brief description of the features of the ignimbrites that were originally mapped as separate ignimbrites (Fig. 2) and classifies the ignimbrite sections into extracaldera or intracaldera facies. As a result of the new correlations, the areal extent of outcrops assigned to the Vilama ignimbrite is considerably enlarged (see Figs. 3 to 5).

3.2 Stratigraphy

The new correlation and distribution of the Vilama ignimbrite allow us to reclassify the ignimbrite deposits on the basis of their stratigraphic attributes and their position with respect to the interpreted collapse structure (Figs. 3, 4, and 5). Two main types of deposits: intracaldera and extracaldera are described .

3.2.1 Intracaldera deposits

The intracaldera deposits comprise the central outcrops of the Vilama ignimbrite (Figs. 3 and 5). They consist of a thick succession of ash-flow deposits that range from a minimum of 400 to 700 meters thick as the base of the sections is unexposed. The deposits constitute an elongated NW-SE-trending (~290º) antiform (Figs. 6A and 6B), which is fairly symmetrical in the NW-SE direction and almost perfectly symmetrical in the perpendicular direction. The ignimbrite sequences appear very homogeneous throughout the outcrop region with no internal sub-blocks with sudden thickness changes. The intercalated lahars in the ignimbrites mentioned by Almendras and Baldellón (1996) in mapping the region were not observed in the field.

The ignimbrites assigned to the intracaldera sequence are moderately to densely welded, massive, and frequently indurated and altered by vapor-phase alteration. Vitrophyric portions usually occur at the base of the outcropping section, although they can also be intercalated in the upper part. Several vitrophyric deposits in the basal levels show a conspicuous jointing that is sometimes subvertical (Fig. 7A) or folded. These joints are interpreted to result from rheomorphic flow. The individual thicknesses of flow units can be as little as 10-20 m, although thicknesses of ~40-50 m are common in the vitrophyres and densely welded tuffs.

As is commonly the case in welded ignimbrites, pumice fragments and lithic clasts are difficult to recognize. Where they can be distinguished, lithic fragments are scarce (<1-5 %) and small (< 12 cm long). They are dominantly sedimentary rocks from the Ordovician basement, and subordinately dacitic lavas. Pumice fragments or fiamme, where they can be identified in less-welded regions, range from rare to abundant (5-20%), are usually large (up to 45 cm) and crystal-rich, and show varying degrees of flattening and welding.

The intracaldera facies of the Vilama ignimbrite are similar to the caldera fill of collapse structures from nearby centers (e.g. La Pacana, Gardeweg and Ramírez, 1987; Lindsay et al, 2001a), or those in other parts of the world (e.g. La Garita caldera, Steven and Lipman, 1976; McDermitt caldera, Hargrove et al., 1984).

3.2.2 Extracaldera deposits

The Vilama ignimbrite outcrops that surround the intracaldera deposits (Figs. 3 and 5) are assigned to the outflow facies. These extracaldera rocks are predominantly pyroclastic flow deposits showing varying degrees of welding. Rare fall and surge deposits also occur. The outflow can be divided into the two distinct cooling units shown in Figure 6C based on their field characteristics. The most diagnostic features are: (1) definable contacts between units, (2) overall induration and welding profiles, (3) aspect ratio, and (4) continuous versus abrupt thickness variation patterns in interpreted transport directions.

(1) Lower cooling unit (LCU)

The LCU can be seen in the area of sections 1 and 4 to the east and southeast of Cerro Salle volcano, in sections 8 and 9 to the south of Cerro Tinte, and in site 26 to the southwest of Laguna Chojllas (Fig. 3). The lower contact of the LCU covers the ~10.25 Ma (Table 3) Lagunillas ignimbrite in section 1, and undated sanidine-rich rhyodacite tuffs in sections 8 and 9. The lower LCU also mantles the 9.8 ± 0.7 Ma (see Table 3) Ojo de Perico dacite lavas north of section 26. The contact between the LCU and the upper cooling unit (UCU) is sharp and erosive as can be observed in sections 1 and 4, east of Cerro Salle (Fig. 3).

The LCU is predominantly formed by massive ignimbrites, although surge (site 1) and fall (site 9) deposits are sparsely intercalated in some localities. Pyroclastic flow deposits are generally unwelded (Fig. 7B), but flattening of pumice and weak welding can be seen in sections 1 and 4, east of Cerro Salle and sections 8 and 9, south of Cerro Tinte. A single welding profile in the region of Cerro Tinte consists of a central sintered section with subtle eutaxitic textures that is gradationally separated from an unwelded base and top.

The massive LCU deposits are gray in color and have high (15-20%) to low (2-3%) amounts of pumice. Individual pumice fragments can be up to 30 cm long in pumice concentration zones. Lithic fragments are scarce (< 1%) and small (< 2 cm long). Deposits near Laguna Chojllas (site 26, Fig. 3 and 7B) are distinctive in having a high proportion of lithics (3-5 %) and pumice (40-50%) and in containing the coarsest fragments in the unit (lithics up to 35 cm long; pumice to 47 cm long). In sections 8 and 9 (Fig. 3), two distinct pumice types occur. The most common is a white to light gray, silky crystal-rich pumice that is porphyritic, has large vesicles and contains crystals up to 5 mm in diameter. The other pumice is banded, light gray to reddish and crystal-poor. This pumice contains smaller vesicles and fragmented crystals (< 2 mm).

The total thickness of the LCU is extremely variable ranging from 7 m to more than 110 m. Judging from the absence of the LCU in places where the UCU directly mantles older units, the LCU is less regionally extensive than the UCU (Figs. 3 and 5). The actual distribution of the LCU is unclear due to possible cover by the relatively uneroded UCU.

Abrupt thickness variations over short distances (e.g., 7 m in section 1 compared to a minimum of 80 m in section 4 whose the base is unexposed, Fig. 3) and an apparent discontinuous extent suggest that the LCU was deposited over a rough pre-existing topography.

(2) Upper cooling unit (UCU)

The UCU is the most extensive and ubiquitous part of the Vilama ignimbrite outflow. The only section where the UCU is unobserved is site 26, southwest of Laguna Chojllas (Figs. 3 and 5). The overall distribution and continuity of the UCU indicate that it was distributed over a relatively flat paleosurface (Fig. 6C).

The UCU consists of a single ignimbrite sheet whose thickness varies uniformly to the north and south from vicinity of the central intracaldera facies. In Argentina, where the base of the UCU is observed, the thickness shows a steady variation (Fig. 3) from ~60 m in the north (section 6) to 18 m in the south (section 11). In Bolivia, the base is observed only in the most distal sections (site 21). There, the UCU is somewhat thinner (~5 m) than in Argentina at a comparable distance from the central caldera facies (e.g. at section 11).

The UCU is a typical low aspect ratio ignimbrite (Walker, 1983) that shows no intercalations with other deposits. Overall, the ignimbrite exhibits a marked variation in color and degree of welding from bottom to the top. Distinctive basal and upper UCU sections are described below.

(a) Basal section (UCUb):

The basal levels of the UCU are the most strongly welded portions of the outflow sheet. The UCUb level is the only part of the UCU that crops out northwest of Laguna Chojllas (Figs. 3 and 5) in the region nearest the topographic rim of the caldera (Fig. 6D). Complete UCUb sections are exposed east of Cerro Salle and south of Cerro Tinte (sections 1 and 8–9, respectively; Fig. 3) where they show maximum thicknesses of ~25 m. The sequences at sites 8 and 9 begin with a densely welded, massive, lithic-free ignimbrite that is 1 to 8 m thick. The fiamme (< 4 cm long) in them are barely distinguishable due to their paucity and extreme welding, and the welding is so extreme that the deposit becomes a black- to reddish brown vitrophye (Fig. 7C). Outcrops near Cerro Salle (site 1) are less welded. The lowermost vitrophyric parts of the UCUb seem to be only locally present. The upper part of the UCUb (6-13 m) develops a tight (1-5 cm thick) contact-parallel jointing (Fig. 6E) as the vitrophyric aspect is gradually lost over a transition zone of several meters (Fig. 7C). This portion of the ignimbrite is brownish gray to purple in color, has small (<3-5 cm) fiamme, and rare to virtually absent (<< 1%) lithic clasts (<1-2 cm long). Sections similar to this part of the UCUb are the most common variant seen in the extracaldera facies of the Vilama ignimbrite.

(b) Upper section (UCUt)

The top part is the least welded part of the UCU, grading from the more densely welded (UCUb) over a short (1-3 m) vertical distance. The UCUt develops an irregular and spaced (>5-20 cm thick) jointing (Fig. 6F) and is typically pink in color, although it can also be light brown. The thickness of the UCUt ranges from 1 to 50 m (Fig. 3). The rock is moderately rich in fiamme (to 10%) and lithic poor (<1%) (Fig. 7D). Pumice fragments are

<5 cm in average length (flattening ratio is 6:1 to 3:1), with maxima lengths up to 35 cm (sections 4, 5, 6 and 10). Lithics are less than 2 cm in length.

3.3 Petrography

The unwelded LCU rocks show vitroclastic textures, in which vitric shards and highly vesiculated pumice are easily identified. In contrast, the more welded UCU varieties show a typical eutaxitic texture with stretched and oriented fiamme, and flattened shards. Shards and fiamme are almost impossible to distinguish in UCUb vitrophyres and the intracaldera facies, where sintering is virtually complete. Glass from the matrix is usually fresh, except in the UCUt and intracaldera facies rocks where the matrix is frequently devitrified into fine quartzo-feldspathic aggregates and/or spherulites.

Pumice fragments are porphyritic, and show the same range of variability in crystal contents as the matrix. UCU fiamme are composed of about 50% crystals. On a vesicle-free basis, the more common LCU pumice has a crystal content of ~35-50%, whereas the rare banded type has 15-20 % crystals. Crystal contents in tuffs are 25-50% in the LCU, and 35-55% in the UCU and intracaldera facies ignimbrites. Crystal contents that lowermost UCUb vitrophyres are 20-41 %.

Primary mineral phases are plagioclase, biotite, quartz, orthopyroxene, hornblende and clinopyroxene (Fig. 8). Accessories phases include apatite, Fe-Ti oxides, zircon and occasionally allanite. The most abundant phenocrysts are plagioclase and biotite grains that can be up to ~3-5 mm long.

The variability in the total crystal content of the pumice and matrix, especially in the outflow UCU and intracaldera facies rocks, seems to correlate with the variability of the relative proportions of the main phenocryst phases (Fig. 8). Increasing relative proportions of quartz and biotite coupled with decreases in plagioclase, hornblende, clinopyroxene and orthopyroxene cannot be simply due to syn-eruptive processes as quartz and biotite should not behave similarly if preferential comminution or winnowing occurred during eruption and transport. The modal variations in the welded deposits of the Vilama ignimbrite are best interpreted as being directly inherited from different parts of a horizontally heterogeneous magma chamber (Soler, 2005). Maughan et al. (2002) used similar arguments to explain phenocryst distributions in the voluminous Lund Tuff (total volume ~3000 km^3).

3.4 Bulk density

Densities of rocks from different facies of the Vilama ignimbrite were measured using a hydrostatic weighing technique in the Department of Physics, Universidad Nacional de Salta (Argentina). Unaltered, non- to weakly-devitrified samples were prepared in ~200 cm^3 cubes, sprayed with an impermeable coating of negligible volume and weight, and then weighed in air and water. Densities of the non-devitrified intracaldera rocks ranged from 2.1 ± 0.2 g/cm^3 (section 13) to 2.29 ± 0.07 g/cm^3 (section 12), depending on the degree of welding.

Densities obtained for LCU samples, as expected from their overall lower degree of welding, were less at 1.28 ± 0.05 g/cm^3 (section 1). Densities of the upper UCU rocks ranged from 2.33 ± 0.06 g/cm^3 (weakly devitrified, section 2) to 2.1 ± 0.1 g/cm^3 (non-devitrified, section 21).

3.5 Biotite chemistry

de Silva and Francis (1989) proposed that the chemical composition of biotites is one of the best fingerprinting elements for correlating extensive ignimbrites in the APVC. This is certainly the case for the Vilama ignimbrite (Table 1). Biotites from the undisputed Vilama ignimbrite have Fe and Mg contents that are more variable than those from other APVC ignimbrites (Fig. 9). Conversely, Ti and Mn contents are very uniform and distinctive. The variability in Fe and Mg, and homogeneity in Ti and Mn contents are also present in ignimbrite units now correlated with the Vilama (Fig. 9). As for the case of variable modal and geochemical compositions (see below), the wide range of Fe and Mg contents in biotites from the redefined Vilama ignimbrite is considered a feature inherited from the Vilama magma (Soler, 2005).

3.6 Whole-rock geochemistry

The whole rock trace and major element analyses of 7 samples from the intracaldera facies and 29 from the outflow facies are plotted in Figure 10 to show the general chemical characteristics of the Vilama ignimbrite. Representative analyses are listed in Table 2, and the full data set is in Soler (2005). Most of the analyses are from welded ignimbrites whose fiamme were too small to separate. Other are of pumices from the unwelded part of the LCU and the UCU (four samples). The compositions of the welded tuffs are considered representative of magma compositions as there are no strong correlation between their chemistry and their modal mineralogy (see Fig. 11; and Soler, 2005). Further evidence comes from the similarities in the ranges of major and trace element concentrations in the tuffs, pumices and fiamme (Fig. 10), and the negligible lithic contents (<1%) in the tuffs.

Chemically, the Vilama ignimbrite is predominantly a high-K_2O calcalkaline dacite with a metaluminous to weakly peraluminous alumina saturation index (molecular $Al_2O_3/CaO+Na_2O+K_2O$) between 0.90 and 1.15 (Fig. 10). Low SiO_2 rhyolitic compositions occasionally occur in the UCUb vitrophyes. The major and trace element compositions of most samples put the Vilama ignimbrite in the 'monotonous intermediate' magma group of Hildreth (1981). The behavior of some trace elements (especially Rb, Sr and Ba) suggests a complex magma chamber history (Fig. 10), which supports the idea of a vertically unzoned, but laterally heterogeneous magma chamber (see Soler, 2005). A detailed discussion of the chemical characteristics of the Vilama ignimbrite will be presented elsewhere.

3.7 Geochronology

Twenty two published and new ages for the Vilama ignimbrite are listed in Table 3. Most of the published ages are for ignimbrite units that have been newly correlated with the Vilama ignimbrite (see Table 1). As a result, eleven new ages are available from the intracaldera and the LCU and UCU extracaldera facies. Three new K/Ar isotopic analyses from Geochron Laboratories (USA) and eight $^{40}Ar/^{39}Ar$ analyses from the Centro de Pesquisas Geocronológicas – USP (Brasil) are presented in Tables 4 and 5. Analytical details are discussed in Appendix A and presented in the supplementary electronic data.

Radiometric ages from the redefined Vilama ignimbrite show a mean age between 8.4 and 8.5 Ma (Table 3). However, some dated samples have yielded ages that are quite different from this mean. For example, sample M-171 from the intracaldera facies yielded K/Ar biotite ages of 8.6 ± 0.9 Ma and 13.1 ± 0.3 Ma (Table 3), as well as the $^{40}Ar/^{39}Ar$ biotite ages (multiple crystal clusters) of 5.4 ± 0.5 Ma (plateau age) and 33.5 ± 0.4 Ma (average of integrated ages) reported in Tables 4 and 5. Disparate published K/Ar dates also occur in ignimbrites now correlated with the Vilama UCU. In particular, the ex-Tobas Lagunillas 1, which has a biotite date of 12.4 ± 0.4 Ma, shows no lateral disruption with the ex-Tobas Lagunillas 3 ignimbrite that has biotite ages of 9.2 ± 0.3 Ma, and 9.0 ± 0.6 Ma (Tables 1 and 3). Further, a pumice sample (M-233p) from an intracaldera tuff from the same location as one with a reported K/Ar age of 10.2 ± 1.1 Ma (Table 3; Almendras and Baldellón, 1996) yielded a $^{40}Ar/^{39}Ar$ plateau age (multiple crystal cluster) of 8.46 ± 0.14 Ma (Tables 3 and 4).

All of these discordant ages are from bulk matrix biotites. As such, the disparate ages could be explained by incorporation of older xenocrystic biotite grains or by a ^{40}Ar excess in the Vilama magma. ^{40}Ar excesses, like those seen in the low temperature steps of some of the Ar/Ar spectra in this study (see supplementary electronic data), have previously been reported in the Vilama and other large-volume APVC ignimbrites (e.g. Sifon) by Tomlinson et al. (2004). These authors concluded that old and scattered biotite K/Ar and $^{40}Ar/^{39}Ar$ dates (compared to ages in other K-rich phases) are best attributed to preferential incorporation of excess radiogenic argon into biotite from the magma. A similar logic can be used to explain the scatter in the ages in Tables 3 to 5. As such, the age discrepancies do not violate the ignimbrite correlations, and the statistically most probable age of the Vilama ignimbrite remains at 8.4 – 8.5 Ma.

Further evidence that the disparate K/Ar ages can be explained by excess Ar or xenocrystic biotite comes from paleomagnetic evidence. In particular, all of the outcrops ascribed to the redefined Vilama ignimbrite, and especially those assigned to the outflow deposits, have similar paleomagnetic properties as shown by Soler et al. (2005). These same paleomagnetic data are consistent with the coeval deposition of the entire Vilama unit during a short-lived eruption. The strong paleomagnetic unity of the Vilama ignimbrite is fully compatible with our correlations based on firm stratigraphic and mineral chemistry grounds (e.g. Table 1).

The appearance of geochronological discrepancies reinforces the importance of detailed field, mineralogical (Hildreth and Mahood, 1985; de Silva and Francis, 1989; Lindsay et al., 2001) and paleomagnetic studies (Somoza et al., 1994; Somoza et al., 1999), and highlights the dangers of relying on age data alone in order to correlate extensive ignimbrites of the APVC and elsewhere.

4. Re-evaluation of the Vilama caldera

4.1 Eruptive source: location and characteristics of the Vilama caldera

The almost complete enclosure of the Vilama intracaldera facies by the outflow sheet and the lack of lateral continuity between these two facies constrain the position of the subsided block to be roughly within the limits of the intracaldera facies outcrop (Fig. 5). This region was formerly interpreted as a resurgent dome by Coira et al. (1996), and as a possible resurgent caldera by de Silva (1989b). The redefined Vilama ignimbrite extracaldera facies can also be used to identify transport direction and better refine the location of the eruptive source.

The most important properties of the extracaldera deposits in constraining the position of the eruptive source are thicknesses and grain sizes in the LCU and UCU. In this regard, the thicknesses of the LCU facies cannot be readily used in determining transport direction as these deposits are interpreted to have erupted over an uneven paleotopography (Fig. 3). In terms of grain size, the coarsest (most proximal) LCU facies lie immediately southwest of the intracaldera deposits (Fig. 5). The rest of the LCU consists of finer grained (more distal) components.

The low aspect ratio, extensive distribution, and excellent continuity make the thickness of the UCU a good indicator of the source position (Fig. 3). The case is particularly strong in Argentina where complete sections are found and thicknesses are seen to vary from north to south. UCU thicknesses are more problematical to the north in Bolivia as the UCUb is unexposed nearest the intracaldera deposits (sites 14, and 15, Fig. 3). However, in that place the UCUb is likely to be present under the UCUt as it is exposed to the north where the UCUt has been removed by erosion (e.g. section 20). The UCU also shows a definite increase in the size of pumice fragments and a slight increase in the size and proportion of lithic fragments towards the inferred subsided block.

Whereas the position of the source is relatively clear, the exact location and geometry of the subsidence structure are more ambiguous. The topographic rim of the Vilama caldera can only be directly observed in the western sector of the inferred subsided block where the 9.8 ± 0.7 Ma Ojo de Perico lavas (Table 3) are dissected by a 250 to 400 m high escarpment (Figs. 3, 4, 5 and 6D). In segments to the north, east and south, the topographic border of the subsided block is almost completely hidden under younger volcanic rocks (Figs. 3 and 4) and the extent of collapse is not visible.

Likewise, the structural margin of the Vilama caldera cannot be outlined unambiguously as it is completely concealed by younger rocks (post-collapse volcanic rocks and caldera moat infill; Fig. 4). At the western margin where the topographic rim can be seen, the structural rim is covered by moat deposits at Laguna Chojllas (Fig. 6D). The position of the western margin can be located with some confidence at 1 to 2 km from the caldera wall (Fig. 4 and 5). Along the rest of the perimeter of the subsided area (Fig. 5), the presence of segments of a structure can only be inferred from indirect evidence that is outlined below. Although this evidence supports a structure around a considerable part of the subsided block, the actual extent and continuity along the inferred segments remain uncertain.

The first line of evidence for the position of the structural margin is that the Vilama ignimbrite shows a wide and equal spread at the same run-out length (~ 40 km, Fig. 5) both to the north and south. This observations suggests that large parts of the northern and southern rims of the subsided area behaved similarly during the collapse. The most logical explanation is that faults with similar displacements existed along the northern and southern sides. Shorter run-out lengths to the east could correlate with a less well developed fault on that side.

The second line of evidence for the position of the structural margin comes from the abrupt changes in thickness (from 60 m to > 400 – 700 m) and inclination that occur between the intracaldera and extracaldera deposits around most of the resurgent dome. The lateral discontinuity between these facies is best attributed to faults at, or very close to the structural rim that were reactivated during later doming. In other calderas (e.g. Lipman, 2000; Cole et al., 2005), the position of the structural margin has often been refined by the location of post-caldera volcanism that preferentially takes place along fractures at the structural border. If post-caldera centers, particularly those emplaced between the intra- and extracaldera facies of the Vilama ignimbrite, represent the location of the structural margin, this margin can be traced along a line that joins the Khastor domes on the west-northwest side of the caldera, the Khastor stratovolcano on the north, the Vitichi and Cerro Bayo domes on the south (Figs. 3 and 4), and the Alcoak and Cerro Salle stratocones on the east.

A caldera moat is well developed around most of the resurgent dome, lying at 4500-4600 masl or about 400 to 800 m below the peaks of the uplifted intracaldera block. In part, the moat coincides with the current position of the Lagunas Chojllas and Coruto, and the Laguna Vilama salar (Figs. 3 and 4). The moat is missing on the easternmost side of the caldera, near the Salle and Alcoak stratovolcanoes (Figs. 3 and 4). Moat deposits are represented by sediments which mainly result from the erosion of the resurgent intracaldera block. Some parts of the caldera moat (e.g., Laguna Coruto; the northeastern edge of Laguna Vilama) are considered to be covered by the younger ignimbrites (see below) that also surround or onlap the Vilama resurgent dome (Fig. 4).

The revised characteristics of the Vilama caldera lead to the new model discussed below in which the Vilama ignimbrite erupted in a single event associated with caldera collapse. The subsided area, which has central coordinates at 66°57'W and 22°24'S, has an elongated shape and stretches in a NW-SE direction. The major axis is ~35-40 km long, and minor axis is ~15-18 km long. The name, Vilama caldera, is retained for the reinterpreted caldera structure as the Laguna Vilama is a salar lake that lies in the moat of the caldera.

4.2 Pre- and post-collapse geology of the Vilama caldera region

4.2.1 Pre-caldera units

Rock units below the Vilama ignimbrite consist of pre-upper Miocene volcanic and sedimentary sequences (Fig. 4). Although these units do not crop out in direct contact with the ignimbrite, they logically constitute the main body of the collapsed block. The principal pre-upper Miocene units include the Paleozoic marine sedimentary Acoite Formation (Turner, 1964), Cretaceous continental and marine rocks of the Salta Group (Salfity and Marquillas, 1994), and Oligocene to middle Miocene volcano-sedimentary sequences (Pacheco and Ramirez, 1997; Coira et al., 2004, and references therein). Pre-caldera upper Miocene andesitic to dacitic ignimbrites and lavas (Fig. 4) units relevant to the discussion of the Vilama caldera with ages in Table 3 are the Lagunillas ignimbrite (10.25 ± 0.12 Ma) to the east of Cerro Salle; the Ojo de Perico lavas (9.8 ± 0.7 Ma) immediately to the west of the intracaldera deposits; the Granada ignimbrite (9.7 ± 0.09 Ma) to the southeast of Cerro Salle; and the undated sanidine-rich and biotite-rich ignimbrites and volcaniclastic rocks (> 8.5 Ma; Soler, 2005; Caffe et al., 2006) that underlie the Vilama ignimbrite outflow facies to the north (biotite-rich) and south (sanidine-rich and biotite-rich).

4.2.2 Post-collapse units

Following the Vilama ignimbrite eruption, a series of domes and stratocones were emplaced in the collapsed area along structures that are interpreted above as being associated with caldera subsidence and resurgence (Figs. 3 and 4). Alternatively, this volcanism could have been channeled along fractures that formed in response to the stress field associated with the subvolcanic magma system (e.g. Bacon, 1985).

According to published ages in Table 3, most of the post-collapse volcanic activity closely followed the Vilama ignimbrite eruption. Among the relevant centers are the Khastor 1 (8.1 ± 0.5; 7.6 ± 0.5 Ma) and Khastor 2 domes (7.6 ± 0.6 Ma), and the Khastor stratovolcano (5 to 8 Ma; García, 1997) that were emplaced along the northern and northwestern segments of the caldera. The Alcoak volcano (6 to 8 Ma; Almendras and Baldellón, 1996), the Cerro Salle stratovolcano (8.4 ± 0.6 Ma), the Toloma and Vilama lavas (<8.4 Ma; Soler 2005), and the Bayo dome (7.49 ± 0.35 Ma) were emplaced in the eastern sector. Near the eastern margin inside the intracaldera block, the subhorizontal Mesada Negra lavas (<8.4 Ma; Almendras and Baldellón, 1996; Soler 2005) unconformably overlie tilted ignimbrites of the Vilama intracaldera facies. These lavas provide a clear example of crestal extrusion in a resurgent dome (Acocella et al., 2004). The Vitichi domes (Pliocene; Almendras and Baldellón, 1996) occur on the south-southwestern side of the caldera. Most of these centers have dacitic compositions. Andesitic centers include the Alcoak volcano, Vilama lavas and Bayo dome. The mineral assemblages of rocks from all these centers are like the Vilama ignimbrite, with most containing ubiquitous biotite and pyroxenes and minor hornblende.

Profuse post-caldera volcanism unrelated to the Vilama system partially covers the Vilama extracaldera sequence, the structural margin, and fills part of the caldera moat (Figs. 3 and 4). Examples of these centers include the Loromayu stratovolcano lavas (6.2 ± 0.5 Ma); the Cienago and Cerro Panizos ignimbrites (6.7 -7.9 Ma) which onlap the resurgent dome at its northeastern sector; and the Bonanza ignimbrite of 6.2 ± 0.5 Ma (Table 3), which cover part of the moat at Laguna Coruto and also onlaps the updomed intracaldera sequence in its southern border.

5. Discussion

5.1 Vilama ignimbrite volume estimate

With the redefinition of the Vilama ignimbrite it is now possible for the first time to calculate reliable volume estimates.

The Vilama ignimbrite outcrops cover an area of ~4000 km^2, spreading out almost equally to both sides of the Argentina-Bolivia border. Since the ignimbrite also filled up a caldera, it is necessary to calculate outflow and intracaldera volumes separately.

5.1.1 Extracaldera volume

The current area covered by the outflow sheet is ~3400 km^2. This area can be conservatively extended to ~6250 km^2 by assuming a continuity in the current outcrops under younger volcano-sedimentary cover (Fig. 5). Given a mean thickness of 40 m, the outflow volume is then 136 to 250 km^3. Even this calculation is probably a minimum, since it is difficult to evaluate how much material has been eroded, and what the real extent of the Vilama ignimbrite is below the young volcanic cover (Figs. 3 and 4).

5.1.2 Intracaldera volume

The method of Lipman (1997) is used below to calculate the volume of the caldera fill. In addition to the parameters explained in Appendix B, the shape and size of the subsided block, the collapse type and the collapse depth are needed. Because of the superficial level of exposure of the Vilama caldera fill and the need to infer the position of the structural border, the values used for these parameters need to be discussed in detail below.

(a) Caldera shape

Taking into account the geometry of the inferred structural border, the map view shape of the Vilama caldera can be approximated as a rectangle whose dimensions are ~35-40 km long, and ~15-18 km wide (Figs. 3 and 5). The average area of collapse is then set at 550 km^2.

(b) Collapse geometry

The geometry of the collapse is not easy to constrain as only the upper 400 to 700 m of the caldera fill sequence (Figs. 6A and 6B) can be seen, landslide breccias are absent, and the caldera floor is not observed. As such, there is no direct way to say if the floor foundered as a single symmetrical (piston-like) or asymmetrical (trap-door-like) block, or as multiple smaller dimension blocks (piecemeal type).

The presence of rheomorphically deformed ignimbrites at the base of the exposed caldera infill does suggests that steep enough slopes favoured post-depositional flow and deformation of high-grade ignimbrites. However, this observation alone is not sufficient evidence that individual blocks acted independently. Additionally, a piecemeal collapse does not seem consistent with resurgent doming exposing the caldera infill as a uniform ignimbrite sequence, rather than as separate blocks with sudden thickness and/or facies changes (Branney and Kokelaar, 1994; Moore and Kokelaar, 1998; Ulusoy et al., 2004).

A single-block collapse geometry is also difficult to conclusively prove, as the topographic rim is exposed only on the western side of the Vilama caldera. Indirect evidence discussed above does provide support for a structural rim on the northern and southern sides, but the case for a rim on the eastern side is less clear (no moat formation, shorter runout length of the outflow facies). Taken as a whole, the evidence is consistent with the caldera floor foundering as a single asymmetrically subsiding block with a hinge on the eastern side. The collapse of some other Andean calderas (e.g. La Pacana, Lindsay et al., 2001a) has been modeled like this. Unfortunately, the Vilama caldera cannot be uniquely modeled in this way. The same field evidence can be used to argue for a slightly asymmetric, non-chaotic, multiple-block subsidence involving increasing collapse depths towards the central axis of the caldera (e.g. Milner et al., 2002). Additional morphostructural and geophysical data could help to resolve this issue.

Considering the uncertainties, volume models for possible piston-like, and trap-door type geometries are explored. Together, the models are useful in constraining the probable maximum and minimum volume estimates for the caldera.

(c) Depth of collapse

Following Lipman (1997), an initial estimate of the subsidence depth can be obtained by adding the maximum height of the topographic wall (~0.40 km) to the average thickness of the exposed intracaldera fill (~0.60 km). This estimate of ~ 1 km is certainly too small in the Vilama case as neither the caldera floor, nor the landslide breccias typically found in basal sections of intracaldera sequences, are exposed. To better estimate the collapse depth, the gravity and aeromagnetic study of Miranda et al. (2006) was employed. They used these data to argue for a subsidence depth of ~2.5 to 3 km and a slightly asymmetric collapse to the north, but could not rule out an alternative model combining the caldera fill with an intrusive root. Their value of 2.5 km is chosen as the maximum subsidence depth for the piston model as this depth is comparable to that estimated for other calderas of similar size (e.g. La Pacana, Lindsay et al., 2001a; La Garita, Aira, Crater Lake, and Creede; Lipman, 1997). The depth for the trap door model is set at 1.8 km, which is an average between the maximum collapse depth of 2.5 km and the minimum of 1 km that is set by the observed outcrop geometry.

The alternative models for the Vilama caldera collapse are then a piston-like collapse with a total subsidence depth of 2.5 km, and a trap-door-like collapse with an average depth of 1.8 km. The area of the collapse is 550 km^2, which is equivalent to the area calculated from the inferred structural rim. The piston-like model gives a total structural volume of 1379 km^3, which includes an intracaldera tuff fill of 1184 km^3. The rest is the unfilled portions of the caldera, and collapse breccia 'lithic fill' (Appendix B). The volume of the intracaldera ignimbrite for the trap-door configuration is 800 km^3.

5.1.3 Total volume

Assuming that the intracaldera block subsided uniformly, an initial estimate of 1434 km^3 is calculated for the Vilama ignimbrite by adding the intracaldera (1184 km^3) and extracaldera (250 km^3) volumes. This is likely an underestimate, since the volume of extracaldera deposits is a minimum. Lipman (1984) suggested that the outflow volume could be estimated by doubling the intracaldera fill. Such a doubling would result in an overestimate in the Vilama case, as this volume would require extreme amounts of erosion that are inconsistent with the post middle Miocene arid climate of the Puna-Altiplano (Vandervoort et al., 1995).

A better estimate comes from the approach used by Lindsay et al. (2001a) for constraining the La Pacana caldera volume. This method takes into account the volume of the caldera fill and the assumption that collapse started early in the eruptive sequence. Most of the ignimbrite (~2/3) ends up being ponded within the caldera. Assuming that ~1/3 of the erupted volume is outflow, the total volume estimate for a piston-like geometry is 1776 km^3. Although high, this volume is likely as the real extent of the Vilama ignimbrite under the Panizos ignimbrite to the northeast, and the Cerro Guacha caldera ignimbrites to the north is uncertain and probably underestimated (Fig. 4). Further, the actual mean thickness of the Vilama ignimbrite outflow in Bolivia (particularly in the most proximal sections) is likely to be underestimated as the base is unexposed (Fig. 3). The calculation here reliably sets the upper volume of the Vilama ignimbrite at ~1800 km^3. Applying the same assumptions to the trap-door geometry and using a collapse depth of 1.8 km results in a volume estimate of 1200 km^3.

The 1800 km^3 and 1200 km^3 volume estimates for the Vilama ignimbrite convert into dense rock equivalent (DRE) values of ~1400 and ~1000 km^3 respectively. This is due to the high welding grade of most UCU and intracaldera facies rocks, which is consistent with the elevated bulk densities measure in most samples. Since weak devitrification may affect bulk densities (Quane and Russell, 2005), only the densities of non-devitrified intracaldera and UCU samples (averaging ~2.1 g/cm^3) were used in calculating the DRE conversion factor. The reference density for a dense dacite was conservatively set at 2.6 g/cm^3, which translates into a mean conversion factor of 0.8. The high welding grade of most of the UCU and intracaldera facies rocks is consistent with elevated bulk densities.

5.2 Eruption of the Vilama ignimbrite and the collapse of the Vilama caldera

The extremely high crystal (≥50 % in pumice and tuff) and low pumice contents (frequently <10 %), the lack of plinian fall deposits, and the high induration of the Vilama intracaldera facies and outflow sheet (apart from some LCU deposits) are characteristics that are common in other extensive ignimbrites in the central Andes (e.g. Sparks et al., 1985; Ort, 1993; Lindsay et al., 2001a,b; de Silva et al., 2006). This suggests that eruptive mechanisms of the Vilama caldera are not unlike those of other calderas in the region.

An important point is that the main volume of the Vilama ignimbrite appears to reside within the caldera. As discussed by Lindsay et al. (2001a), this situation is better understood if the collapse of the caldera started early in the eruptive history. A relatively early onset of collapse for the Vilama caldera, and continued subsidence until the end of eruption are consistent with the lack of plinian fall deposits and the high degree of welding and induration in most of the outflow sheet and intracaldera deposits. These characteristics, along with high crystal and low pumice contents, and the low aspect ratio in the UCU support deposition from dense and hot pyroclastic flows, that in turn formed from continuous collapse of low and unstable eruptive columns, i.e. as boiling over collapse fountains (Branney and Kokelaar, 1992; Branney and Kokelaar, 1994; Freundt, 1999).

The high eruption rates needed to produce boiling over collapse fountains are best achieved when the caldera floor sinks into the magma body, causing the magma to be evacuated rapidly through bounding faults. This dynamic is consistent with eruption and magma withdrawal being controlled by an external drive, rather than simply by violent release of volatiles from the magma. Subsidence driven eruption processes like this have been proposed for other Central Andean calderas with large-volume ignimbrites like the Vilama (Sparks et al., 1985; Schmitt, 2001; Lindsay et al., 2001a,b).

The evidence supporting caldera collapse by the withdrawal of the Vilama magma is clear, but the eruption trigger is not. A recent model by de Silva et al. (2006) suggests that the most likely trigger for Andean calderas is not produced by magmatic overpressure, but by the mechanical failure of magma chamber roofs. This process is thought to be intimately associated with several million years of thermal softening of the upper crust by an enhanced thermal flux. This flux causes the wall rocks to behave ductilly and the magma chambers to grow extensively without erupting (also see Jellinek and de Paolo, 2003). This mechanism can also satisfactorily explain many of the features of the Vilama ignimbrite including its large-volume, petrographic and stratigraphic characteristics and eruption dynamics.

An eruption triggered by instability of the magma chamber roof is also consistent with the almost rectangular shape that has been inferred for the Vilama caldera (Figs. 3 and 5). Notably, the northwest-oriented caldera (Fig. 4) is elongated in the same direction as left-lateral faults along the Lipez Lineament. This parallelism is consistent with the regional tectonic framework exerting some kind of control over the caldera shape (e.g. Viramonte et al., 1984; Petrinovic, 1999; Riller et al., 2001). Given visco-elastic conditions, it seems unlikely that transtensional/distensive stresses alone triggered the collapse of the caldera as tectonic strain rates would have been too low (Jellinek and DePaolo, 2003). More likely, tectonic stresses caused the Vilama magma chamber to develop parallel in extension direction, or pre-existing regional faults influenced the final shape of the subsided block (Acocella et al., 2004).

5.3 Model for the Vilama caldera

Figure 12 shows an interpretative model for the collapse and resurgence of the Vilama caldera. In the model, the main Vilama ignimbrite eruption is envisaged as a complex volcanotectonic process that led to catastrophic collapse of the chamber roof, and evacuation of a large part of the Vilama magma chamber.

The eruption of the LCU, which is the lower part of the outflow, is interpreted to require different conditions from those of the main eruption as shown in Figure 12A. Based on its overall lower degree of welding, and the presence of fall and surge deposits in distal outcrops, the LCU probably formed from well-developed eruptive columns with more efficient convective phases (Cas and Wright, 1987; Cioni et al., 2000). The eruption likely involved the release of magmatic overpressures from a more-volatile enriched magma cap than was present later at the time of the main eruption. From a volume perspective, the eruption of the LCU seems too small to have been an effective trigger for collapse of the entire roof of the Vilama magma chamber. Instead, the volcanic plumes that produced the LCU are interpreted to have formed immediately before or at the beginning of the main collapse when subsidence faults were incipient, and volcanic discharge rates and the dimension of initial vents were small (Bursik and Woods, 1996; Legros et al., 2000). As a result, the LCU ignimbrites were the first to erupt and form the base of the outflow facies.

Once the structures on which the main subsidence occurred were well developed, conditions changed, and the eruption of the main portion of the outflow (UCU) facies and intracaldera deposits began as shown in Figures 12B and 12C. The low aspect ratio of the UCU, the high welding grade, the crystal-rich and pumice-low nature and the virtual absence of other types of interfingered deposits are all consistent with boiling-over collapse fountains forming along caldera bounding faults at this time. The volcanic plumes collapsed preferentially towards the downthrown side of the faults bounding the caldera, causing the largest portion of the Vilama ignimbrite to be ponded within the caldera.

The period between the caldera collapse and resurgence was apparently short (< 1 Ma) as shown by the difference in the average age of the Vilama ignimbrite (8.4-8.5 Ma) and post-caldera (mostly effusive) volcanism (Table 3). This time frame is consistent with the eruption being driven and sustained by collapse of the magma chamber roof, rather than magmatic overpressures, during the main collapse stage. A relatively fast recovery of post-collapse magmatic pressures (Figs. 12C and 12D) can explain related effusive eruptions within a short period of time. Some of the intracaldera deposits were domed and peripheral and crestal lavas (Figs. 3 and 12D) were extruded through extensional fractures in the final stages of the Vilama caldera. The shape of the resurgent dome is similar to that modeled by Acocella et al. (2001) for caldera resurgence associated with a shallowly intruded, large-volume, planar magma chamber with a roof aspect ratio ~0.4.

6. Conclusions

The characteristics of the Vilama ignimbrite have been redefined, leading to recognition of intra- and extracaldera facies deposits. Based on correlations of ignimbrites that were previously mapped as individual units, the areal extent of outcrops ascribed to the Vilama ignimbrite is over 4000 km^2. The average crystallization age for the ignimbrite is 8.4-8.5 Ma with older discordant ages being interpreted as reflecting excess ^{40}Ar in biotite or contamination with xenocrystic mica. The Vilama ignimbrite erupted from the Vilama caldera which is defined as a collapse structure with a roughly rectangular structure in map view, a major axis of ~35-40 km directed to the northwest, a minor axis of ~15-18 km, and central coordinates of 66°57’W and 22°24’S. The topographic rim of the caldera is visible in the western sector, and a structural border can be inferred along a considerable part of the perimeter surrounding the intracaldera outcrop. Due to the poor exposure of the topographic rim, the extent of collapse and the overall geometry of the caldera subsidence are incompletely known. Possible models include a slightly asymmetric single-block subsidence, or an asymmetric or symmetric non-chaotic multiple-block collapse. Volume estimates for the Vilama ignimbrite range from a maximum for a symmetric collapse of 1800 km^3 (~1400 km^3 DRE), to a minimum of 1200 km^3 (~1000 km^3 DRE) for an asymmetric subsidence. These estimates class the Vilama caldera eruption as one of the largest described super explosive volcanic events on Earth.

In accord with the petrographic and stratigraphic characteristics of the Vilama ignimbrite and its prodigious erupted volumes, an external driving force other that volatile overpressure seems to have controlled and maintained the eruption without significant change until the end. As in other large-volume Andean ignimbrites, the most likely cause is caldera subsidence, which can induce a large volume of magma to be withdrawn from a batholith-scale magma chamber in a short time. Eruption was likely triggered by roof chamber instability (de Silva et al., 2006), facilitated by a planar shape and an extremely large magma volume in an upper crustal subvolcanic reservoir. Extension associated to active or fossil left-lateral faults may have exerted some control on the northwest elongated shape of the caldera and the final subelliptical/rectangular shape of the subsided block (e.g. Acocella et al., 2004).

The first pyroclastic flows erupted from the Vilama caldera deposited the extracaldera Vilama ignimbrite lower cooling unit (LCU) over a pre-existing irregular topography. This ignimbrite originated by collapse of relatively high eruptive columns with efficient convective phases that could have formed immediately before or at the beginning of caldera subsidence. Once the boundary faults developed and the caldera collapse was established, eruptive conditions changed, initiating the emission of the rest of the outflow (the upper cooling unit: UCU) and the intracaldera deposits. During this phase, which lasted until the end of the explosive event, eruptive columns were low and unstable and mostly collapsed towards the inner side of the caldera walls. This caused the largest part of the ignimbrite to be ponded within the caldera. After a short time, volcanic unrest, perhaps linked to recharge of the magma chamber, resulted in the formation of a resurgent dome by folding of the intracaldera sequence. Predominantly effusive post-collapse volcanism characterized the area for the next ~2 Ma.

Acknowledgements

We thank all of the personnel from the Instituto de Geología y Minería (Universidad Nacional de Jujuy, Argentina) and CONICET (Argentine National Council of Scientific and Technological Research) for their professional and technical support, especially R. Liquín, P. Flores, E. Cachizumba, S. Rosas and F. Baysse. We also want to thank G. Lesino and A. Hernández (INENCO, Universidad Nacional de Salta) for density data determinations. Fruitful debates and discussion of ideas about the Vilama ignimbrite geology with R. Somoza, D. Fracchia, A. Diaz, A. Ramírez, J.F. Vilas, A. Tomlinson, and U. Cordani are gratefully acknowledged. This work would have been impossible without the support of authorities and personnel of the two natural reserves in the study area: the Reserva Alto Andina Eduardo Avaroa (Bolivia), and the Reserva Provincial Alto Andina de la Chinchilla (Jujuy-Argentina). We are also thankful for the hospitality of people from the Puna of Jujuy and neighboring areas in southwest Bolivia. M. Soler is gratefully indebted to CONICET for funding part of his PhD Thesis through a doctoral fellowship. Additional funding came from grants PIP-CONICET 2638 to B. Coira, and PICT (ANPCyT) 07-12420, and 07-12376, to B. Coira and P. Caffe, respectively. Thorough and constructive reviews of the original manuscript by R.B. Trumbull, and the Journal referees J.M. Lindsay and S.L. de Silva substantially improved the quality of this work.

Appendix A. $^{40}Ar/^{39}Ar$ and K/Ar methodology

$^{40}Ar/^{39}Ar$ dating (Table 4) was performed on biotite separates in the Ar/Ar facility of the Centro de Pesquisas Geocronológicas – USP (Brasil). Clean and fresh crystals of biotite

(>0.5-<2 mm in diameter), either from pumice or whole-rock, were separated by hand-picking. For the argon extractions, the best grains were selected and mounted in a copper disc for single grain incremental heating analysis (with a 6W Ar-ion laser). In the case of samples M-171, M-233p, and M-258 (Table 4) a multiple grain cluster was mounted. For most samples, the measurements were done in duplicate, and for sample M-194, in triplicate. After heating, the extracted gas was analized in a MAP-215-50 mass spectrometer. The irradiation sessions were carried out at the IPEN/CNEN reactor (USP) and in all cases the standard reference was the FC-2 sanidine (28.02 ± 0.09 Ma; Renne et al., 1998). Further details about equipment of the $^{40}Ar/^{39}Ar$ laboratory at CPGeo, analytical procedures, data collection, and statistical treatment, are described in Vasconcelos et al. (2002). Graphs with all isotopic spectra, and a table with the complete data set, are provided by the journal as supplementary electronic material.

Three new K/Ar (biotite) ages (Table 5) were obtained at the Geochron Laboratories (USA). Biotite (-80/+200 mesh) was separated from the whole-rock because pumice fragments were too small. K_2O (wt. %) concentrations were measured by flame spectrophotometry, the reported values for each sample being the average of two different analyses. ^{40}K (ppm) concentrations were calculated from the terrestrial isotopic abundance, using the measured K_2O concentration. $^{40}Ar^*$ (ppm) concentrations, corresponding to radiogenic ^{40}Ar, were derived using the conventional equation from isotopic dilution measurements on a mass spectrometer, after correcting the value for the presence atmospheric Ar. Reported concentrations represents the average of two different runs for each sample. Radiogenic $^{40}Ar^*/^{total}Ar$, and $^{40}Ar/^{36}Ar$ ratios, were derived from the direct measurement with a mass spectrometer during two different readings, whose results are later averaged.

(Tables 4 and 5)

Appendix B. Volume estimate calculations

(Table 6)

References

Acocella, V., Cifelli, F., Funiciello, R., 2001. The control of overburden thickness on resurgent domes: insights from analogue models. J. Volcanol. Geotherm. Res. 111, 137-153.

Acocella, V., Funiciello, R., Marotta, E., Orsi, G., de Vita, S., 2004. The role of extensional structures on experimental calderas and resurgence. J. Volcanol. Geotherm. Res. 129 (1/3): 199-217.

Almendras, O.A. and Baldellón, E.G.P., 1996. Hoja Laguna Busch/Intihuasi 6126/6226. Carta Geológica de Bolivia, Escala 1: 100000, Publicación SGM Serie I-CGB-42, Servicio Nacional de Geología y Minería.

AQUATER, 1979. Estudio del potencial geotérmico de la Provincia de Jujuy, República Argentina. Secretaría de Estado de Minería de la Provincia de Jujuy (unpublished report): 129 pp.

Bacon, C. R., 1985, Implications of silicic vent patterns for the presence of large crustal magma chambers. J. Geophys. Res. 90: 11243-11252.

Baker, F., Francis, W., 1978. Upper Cenozoic Volcanism in the Central Andes – Ages and volumes. Earth Planet. Sci. Lett. 41 (2): 175-187.

Branney, M.J., Kokelaar, P., 1992. A repppraisal of ignimbrite emplacement: progressive aggradation and changes from particulate to non-particulate flow during emplacement of high-grade ignimbrite. Bull. Volcanol. 54 (6): 504-520.

Branney, M. J., Kokelaar, P., 1994. Volcanotectonic faulting, soft-state deformation and rheomorphism of tuffs during development of a a piecemeal caldera, English Lake District. Geol. Soc. Am. Bull. 106: 507–530.

Bursik, M.I., Woods, A.W., 1996. The dynamics and thermodynamics of large ash flows. Bull. Volcanol. 58 (2/3): 175-193.

Caffe, P.J., Soler, M.M., Coira, B.L., Onoe, A.T., Cordani, U.G, 2006. The Granada ignimbrite: a compound pyroclastic unit, and its relationship with Upper Miocene caldera volcanism in the northern Puna. J. South Am. Earth Sci. (in press).

Caffe, P.J., Trumbull, R.B., Coira, B.L., Romer, R.L., 2002. Petrogenesis of Early Neogene magmatism in the Northern Puna; implications for magma genesis and crustal processes in the Central Andean Plateau. J. Petrol. 43 (5), 907-942.

Cas, R.A.F., Wright, J.V., 1987. Volcanic Successions Modern and Ancient. Chapman & Hall, London. 528 pp.

Choque, N.M., 1996. Hoja Volcán Putana 6026. Carta Geológica de Bolivia, Escala 1: 100000, Publicación SGM Serie I-CGB-41, Servicio Nacional de Geología y Minería de Bolivia.

Cioni, R., Marianelli, P., Santacroce, R., Sbrana, A., 2000. Plinian and subplinian eruptions. In: Sigurdsson, H., Houghton, B., McNutt, S.R., Rymer, H. y Stix, J. (Eds): Encyclopedia of Volcanoes, pp. 477 - 494. Academic Press.

Coira, B., Kay, S.M., Viramonte, J., 1993. Upper Cenozoic Magmatic Evolution of the Argentine Puna - A model for changing subduction geometry. Int. Geol. Rev. 35 (8): 677-720.

Coira, B.; Caffe, P.; Mahlburg Kay, S.; Díaz, A., Ramírez, A., 1996. Complejo Volcánico Vilama-Sistema caldérico del Cenozoico superior en Puna, Jujuy. Actas XIII Congreso Geológico Argentino-III Congreso de Exploración de Hidrocarburos (3): 603-620.

Coira, B., Caffe, P., Ramirez, A., Chayle, W., Diaz, A., Rosas, S., Perez, A., Perez, B., Orosco, O., Martínez, M., 2004. Hoja Geológica Mina Pirquitas 2366-I/2166-III, (1:250.000). Boletín 269 SEGEMAR, IGRM. 123 pp.

Cole, J.W., Milner, D.M., Spinks, K.D., 2005. Calderas and caldera structures: a review. Earth Sci. Rev. 69 (1/2): 1-26.

de Silva, S.L., 1987. Large-volume explosive silicic volcanism in the Central Andes of North Chile. Tesis doctoral. Open University, U.K., 409 pp.

de Silva, S.L., 1989a. Altiplano-Puna volcanic complex of the central Andes. Geology 17 (1/2): 1102-1106.

de Silva, S.L., 1989b. Geochronology and stratigraphy of the ignimbrites from the 21°30'S to 23°30'S portion of the central Andes of norhtern Chile. J. Volcanol. Geotherm. Res. 37 (2): 93-131.

de Silva, S.L, Francis P.W., 1989 Correlation of large volume ignimbrites - two case studies from the Central Andes of N. Chile. J. Volcanol. Geotherm. Res. 37 (2): 133-149.

de Silva, S.L., Francis, P.W., 1991. Volcanoes of the Central Andes. Springer-Verlag, Heidelberg. 263 pp.

de Silva, S.L., Zandt, G., Trumbull, R., Viramonte, J., Salas, G., Jimenez, N., 2006. Large ignimbrite eruptions and volcanotectonic depressions in the central Andes – A thermomechanical perspective. In: de Natale, G., Troise, C., Kilburn, Ch. (Eds.) Mechanisms of activity and unrests at large calderas, Geol. Soc. London Special Publication 269, Chapter 3, 47-63.

Francis, P.W, Baker, M.C.W., 1978. Sources of two large ignimbrites in the central Andes; some Landsat evidence. J. Volcanol. Geotherm. Res. 4 (1/2), 81-87.

Fernández, S.R., 1997. Hoja Volcán Juriques 6025. Carta Geológica de Bolivia, Escala 1: 100000, Publicación SGM Serie I-CGB-46, Servicio Nacional de Geología y Minería de Bolivia.

Freundt, A., 1999. Formation of high-grade ignimbrites Part II. A pyroclastic suspension current model with implications also for low-grade ignimbrites. Bull. Volcanol. 60 (7): 545-567.

García, R.D., 1997. Hoja Geológica Laguna Corante/Picalto 6227/6327. Carta Geológica de Bolivia, Escala 1: 100000, Publicación SGM Serie I-CGB-48, Servicio Nacional de Geología y Minería.

Gardeweg M., Ramírez C., 1987. La Pacana Caldera and the Atana Ignimbrite. A major ash-flow and resurgent caldera complex in the Andes of northern Chile. Bull. Volcanol. 49 (3): 547-566.

Hargrove, H.R., Sheridan, M.F., 1984. Welded tuffs deformed into megarheomorphic folds during collapse of the McDermitt Caldera, Nevada-Oregon. J. Geophys. Res. 89 (10): 8,629-8,638.

Hildreth, W., 1981. Gradients in silicic magma chambers: implications for lithospheric magmatism. J. Geophys. Res. 86 (B11): 10,153-10,192.

Hildreth, W., Mahood, G.A., 1985. Correlation of ash-flow tuffs. Geol. Soc. Am. Bull. 96: 968-974.

Jellinek, A.M., DePaolo, D.J., 2003. A model for the origin of large silicic magma chambers: precursors of caldera-forming eruptions. Bull. Volcanol. 65 (5): 363-381.

Kay, S. M., C. Mpodozis, B. Coira, 1999. Magmatism, tectonism, and mineral deposits of the Central Andes (22°-33°S latitude. In Skinner, B. (Ed.), Geology and Ore Deposits of the Central Andes, Society of Economic Geology Special Publication No. 7, 27-59.

Kretz, R., 1983. Symbols for rock-forming minerals. Am. Mineral. 68: 277-279.

Legros, F., Kelfoun, K., Martí, J., 2000. The influence of conduit geometry on the dynamics of caldera-forming eruptions. Earth Planet. Sci. Lett. 179 (1): 53-61.

Lema, J.C., Ramos, W., 1996. Hoja Zapaleri 6125. Carta Geológica de Bolivia, Escala 1: 100000, Publicación SGM Serie 1-CGB-39, Servicio Nacional de Geología y Minería.

Le Maitre, R.W., 1989. A classification of igneous rocks and glossary of terms. Blackwell Scientific Publications, 193p.

Lindsay, J.M., de Silva, S., Trumbull, R., Emmermann, R., Wemmer, K., 2001a. La Pacana caldera, N. Chile: a re-evaluation of the stratigraphy and volcanology of one of the world's largest resurgent calderas. J. Volcanol. Geotherm. Res. 106 (1/2): 145-173.

Lindsay, J.M., Schmitt, A.K., Trumbull, R.B., de Silva, S.L., Siebel, W., Emmermann, R., 2001b. Magmatic evolution of the La Pacana caldera system, Central Andes, Chile: compositional variation of two cogenetic, large-volume felsic ignimbrites. J. Petrol. 42 (3): 459-486.

Lipman, P.W., 1984. The roots of ash flow calderas in western North America: windows into the tops of granitic batholiths. J. Geophys. Res. 89 (B10): 8801–8841.

Lipman, P.W., 1997. Subsidence of ash-flow calderas: relation to caldera size and magma-chamber geometry. Bull. Volcanol. 59 (3):198-218.

Marret, R., Strecker, M.R., 2000. Response of intracontinental deformation in the central Andes to late Cenozoic reorganization of South American Plate motions. Tectonics 19 (3): 452-467.

Maughan, L.L., Christiansen, E.H., Best, M.G., Grommé, C.Sh., Deino, A.L., Tingey, D.G., 2002. The Oligocene Lund Tuff, Great Basin, USA: a very large-volume monotonous intermediate. J. Volcanol. Geotherm. Res. 113 (1/2): 129-157.

Milner, D.M., Cole, J.W., Wood, C.P., 2002. Asymmetric, multiple-block collapse at Rotorua Caldera, Taupo Volcanic Zone, New Zealand. Bull. Volcanol. 64: 134-149.

Miranda, S., Coira, B., Soler, M., Pacino, M.C., 2006. Subsidencia de la caldera Vilama (Puna argentina – Altiplano boliviano) inferida a partir de datos de gravedad y aeromagnéticos. XXIII Reunión Científica de Geofísicos y Geodestas (AAGG2006). Resúmenes. Bahía Blanca.

Mobarec R., Heuschsmidt, B. 1994. Evolución tectónica y diferenciación magmática de la Caldera de Guacha, sudoeste de Bolivia. Actas VII Congreso Geológico Chileno (1): 112-116. Concepción.

Moore, I., Kokelaar, P. Tectonically controlled piecemeal caldera collapse: a case study of Glencoe volcano, Scotland. Geol. Soc. Am. Bull. 110 (11): 1448-1466.

Ort, M., 1993. Eruptive processes and caldera formation in a nested downsag-collapse caldera: Cerro Panizos, Central Andes Mountains. J. Volcanol. Geotherm. Res. 56 (3): 221-252.

Pacheco, J.Z., Ramírez, V.F., 1996. Hoja Quetena 6127. Carta Geológica de Bolivia, Escala 1: 100000, Publicación SGM Serie I-CGB-40, Servicio Nacional de Geología y Minería.

Pacheco, J., Ramírez, V., 1997. Hoja Soniquera 6128. Carta Geológica de Bolivia, Escala 1: 100000, Publicación SGM Serie I-CGB-51, Servicio Nacional de Geología y Minería.

Petrinovic, I.A., 1999. La caldera de colapso del cerro Aguas Calientes, Salta, Argentina, evolución y esquema estructural. In: Colombo, F., Queralt, I, Petrinovic, I.A. (Eds.) Geología de los Andes centrales meridionales: El Noroeste Argentino. Acta Geológica Hispánica 34 (2-3): 243-253.

Renne, P.R., Swisher, C.C, Deino, A.L., Karner, D.B., Owens, T.L., DePaolo, D.J., 1998. Intercalibration of standards, absolute ages and uncertainties in $^{40}Ar/^{39}Ar$ dating. Chem. Geol. 145 (1/2): 117-152.

Riller, U., Petrinovic, I., Ramelow, J., Strecker, M., Oncken, O., 2001. Late Cenozoic tectonism, collapse caldera and plateau formation in the central Andes. Earth Planet. Sci. Lett. 188 (3/4): 299-311.

Salfity, J.A., Marquillas, R.A., 1994. Tectonic and sedimentary evolution of the Cretaceous-Eocene Salta Group basin, Argentina. In Salfity, J.A. (Ed.): Cretaceous tectonics of the Andes: 266-315. Earth evolution Sciences,. Friedr. & Sohn Braunschweig/Wiesbaden.

Saunders, S.J., 2005. The possible contribution of circumferential fault intrusion to caldera resurgence. Bull. Volcanol. 67 (1): 57-71.

Schmitt, A.K., 2001. Gas-satured crystallization and degassing in large-volume, crystal-rich dacitic magmas from the Altiplano-Puna, northern Chile. J. Geophys. Res. 106 (12): 30,561-30,578.

Seggiaro R., 1994. Petrología, geoquímica y mecanismos de erupción del Complejo Volcánico Coranzulí. PhD Thesis. Facultad de Ciencias Naturales, Universidad Nacional de Salta. 137 pp.

Soler, M.M., 2005. Caldera Vilama (Mioceno Superior): Su Estratigrafía, Evolución Magmática y Relación con Eventos Ignimbríticos Tempranos. Puna Argentina – Altiplano Boliviano. PhD Thesis. Universidad Nacional de Salta. 358 pp.

Soler, M.M., Caffe, P.J., Coira, B., Onoe, A.T., 2005. La Caldera Vilama y el Complejo Caldérico Eduardo Avaroa, Puna argentina – Altiplano boliviano. Actas XVI Congreso Geológico Argentino (1): 673-678. La Plata.

Soler, M.M., Singer, S.E., Tomlinson, A.J., Somoza, R., Raposo, M.I.B., Matthews, S., Perez d´Arce, C., Blanco, N., Vilas, J.F., 2005. Detecting a major ignimbrite event in the Central Andes. 6th Int. Symp. of Andean Geodynamics: 677-678. Barcelona.

Somoza, R., Singer, S., Coira, B., Vilas, J.F., Díaz, A., Caffe, P., 1994. Ignimbritas del complejo volcánico Vilama (22,6°S – 67°O) – Correlaciones paleomagnéticas y petrológicas. Actas VII Congreso Geológico Chileno (1): 179-183.

Somoza, R., Singer, S., Tomlinson, A., 1999. Paleomagnetic study of upper Miocene rocks from northern Chile: implications for the origin of late Miocene - Recent tectonic rotations in the southern Central Andes. J. Geophys. Res. 104 (10): 22,923-22,936.

Sparks, R.S.J., Francis, P.W., Hamer, R.D., Pankhurst, R.J., O’Callagham, L.O., Thorpe, R.S., Page, R., 1985. Ignimbrites of the Cerro Galán caldera, NW Argentina. J. Volcanol. Geotherm. Res. 24 (3/4): 205-248.

Steven, T.A., Lipman, P.W., 1976. Calderas of the San Juan volcanic field, southwestern Colorado. U.S. Geol. Survey Prof. Paper 958, 35 pp.

Tomlinson, A.J., Matthews, S., Perez d’Arce, C., Soler, M., Blanco, N., Somoza, R., Singer, S., 2004. False $^{40}Ar/^{39}Ar$ plateaus, meaningless inverse isochrons and excess ^{40}Ar from the Late Miocene Sifón and Vilama Ignimbrites, south Central Andes, 21°30’-23°S: Obstacles for an accurate chronology in silicic ignimbrite sequences. IAVCEI General Assembly, Abstracts CD-ROM, Pucón, Chile.

Turner, J.C.M., 1964. Descripción geológica de la Hoja 2c Santa Victoria (Provincias de Salta y Jujuy). Boletín del Instituto Nacional de Geología y Minería 104, 83 pp.

Ulusoy, I., Cubucku, E., Aydar, E., Labazuy, P., Gourgaud, A., Vincent, P.M., 2004. Volcanic and deformation history of the Bodrum resurgent caldera system (southwestern Turkey). J. Volcanol. Geotherm. Res. 136: 71-96.

Vandervoort, D.S., Jordan, T.E., Zeitler, P.K., Alonso, R.N., 1995. Chronology of internal drainage development, and uplift, southern Puna plateau, Argentine central Andes. Geology 23 (2): 145-148.

Vasconcelos, P.M., Onoe, A.T., Kawashita, K., Soares, A.J., Teixeira, W., 2002. $^{40}Ar/^{39}Ar$ geochronology at the Instituto de Geociências, USP: instrumentation, analytical procedures, and calibration. Anais de Academia Brasileira de Ciências 74 (2): 297-342.

Viramonte, J.G., Galliski, M.A., Saavedra, V.A., Aparicio, A., García-Cacho, G.L., Escorza, C.M., 1984. El finivulcanismo básico de la depresión de Arizaro, provincia de Salta. Actas IX Congreso Geológico Argentino (3): 234-251.

Walker, G.P.L., 1983. Ignimbrite types and ignimbrite problems. In: M.F. Sheridan and F. Barberi (Eds.), Explosive Volcanism. J. Volcanol. Geotherm. Res. 17 (1/4): 65-88.

Figure captions

Figure 1. Map of outcrops of late Neogene ignimbrites (modified from Lindsay et al., 2001a) in the Central Volcanic Zone; the position of the main volcanic arc is also shown. Caldera structures which presumably sourced large-volume ignimbrites are highlighted. The approximate extent of the APVC (Atiplano Puna Volcanic Complex) is modified from de Silva (1989a). The inset shows the four active volcanic zones of the Andes.

Figure 2. Map of the distribution of Granada and Vilama ignimbrites, their inferred flow directions, and the limits of the Vilama caldera following the interpretation of Coira et al. (1996). Also indicated are other ignimbrites that were previously mapped as separate units, but which are now correlated with the Vilama ignimbrite (see Table 1 and text).

Figure 3. Satellite image of the study area (Landsat TM) with location of the 27 stratigraphic sections studied in the Vilama ignimbrite outcrop area. Newly defined sub-units of the Vilama ignimbrite, as well as volcanic rocks that underlie or overlie them, are shown for each section. Geographic coordinates of all stratigraphic sites are given in the lower left corner. The political boundary between Argentina, Chile and Bolivia (dashed black line), as well as the new location and some features of the reinterpreted Vilama caldera (continuous white line: exposed topographic rim; dashed white line: inferred subsided block) have been marked. VC: Vilama caldera; KD: Khastor domes; KS: Khastor stratovolcano; AS: Alcoak stratovolcano; CSS: Cerro Salle stratovolcano; TL: Toloma lavas; VL: Vilama lavas; BD: Bayo dome; MNL: Mesada Negra lavas; VD: Vitichi domes; VS: Vilama stratovolcano; CT: Cerro Tinte stratovolcano; LgCH: Laguna Chojllas; LgC: Laguna Coruto; LgV: Laguna Vilama.

Figure 4. Geological map of the Vilama caldera area, with the interpreted position of the subsidence structure and redefined distribution of the Vilama ignimbrite outcrops. Numbered circles correspond to sites with radiometric dates, either from this or previous work (numbers correspond with those in Table 3). AGVC: Abra Granada Volcanic Complex. AS: Alcoak stratovolcano. CSS: Cerro Salle stratovolcano. KS: Khastor stratovolcano. KD: Khastor dome. VD: Vitichi domes. VS: Vilama stratovolcano. BD: Bayo dome. The location of other caldera structures is from de Silva (1987); Mobarec and Heuschmidt (1994); Almendras and Baldellón (1996); Lema and Ramos (1996); Choque (1996); Fernández (1997); Ort (1993); and Seggiaro (1994).

Figure 5. Sketch map with the new distribution of the Vilama ignimbrite and associated sub-units. The outer rim of the inferred subsided Vilama caldera block is indicated with a dashed line. The minimum (observed outcrops) and enlarged (interpreted) areal extents ascribed to the Vilama ignimbrite are also shown.

Figure 6. Field photographs showing the Vilama ignimbrite (see section locations in Fig. 3). A and B) Intracaldera facies from sections 13 (view to northwest) and 27 (view to southeast), respectively. The black line shows the flat depositional surface of different flow units in the succession of thick welded and indurated ignimbrites. MNL: Mesada Negra lavas; BD: Bayo dome. C) Vilama ignimbrite outflow sequence to the east of Cerro Salle stratovolcano (CSS), near section 1. Here, the extensive plateau consists of the unwelded lowermost cooling unit (LCU), and the welded upper cooling unit (UCU) displaying a differentiated base (UCUb) and top (UCUt) . D) View to east of the Vilama caldera fill from the top of the topographic wall in the western rim of the caldera. The Khastor dome (KD) is clearly intruded between the intra- (VI-IF) and extracaldera (VI-UCUb) facies of the Vilama ignimbrite. The black line approximately traces the topographic rim. Lch: Laguna Chojllas; OPL: Ojo de Perico lavas. E and F) Outcrops of the Vilama ignimbrite outflow showing the typical subhorizontal jointing that characterizes the base (E; section 19), or the top (F; section 16) of the upper cooling unit.

Figure 7. A) Vitrophyric aspect of an ignimbrite from the intracaldera sequence (section 13; Fig. 3). Note the well developed subvertical jointing due to deformation during rheomorphic flow. B) Outcrop of the lower cooling unit of the Vilama ignimbrite outflow facies to the southwest of Laguna Chojllas (section 26; Fig. 3). The generally low degree of induration, abundant pumice (P) and lithic (L) fragments of moderate to large size are typical

features of this unit at this locality. Hammer is ~ 33 cm long. C) Upper cooling unit base (UCUb) in section 8, to the southeast of Cerro Tinte (Fig. 3). A massive black vitrophyre (white arrow) appears at the base of the section, gradually passing upwards to a reddish brown foliated rock with tight jointing (black arrow), which is the most usual aspect of the UCU. D) Top of the upper cooling unit (UCUt) at section 9 (south of Cerro Tinte, Fig. 3). The general absence of lithic fragments, and the reduced size of fiamme are typical characteristics of this facies of the Vilama ignimbrite. The white arrows indicate fiamme ~ 1 - 3 cm long.

Figure 8. Vilama ignimbrite modal compositions (of the whole-rock, pumice and fiamme). The phenocryst abundances of each mineral phase were measured from point counting (base 1500 points), and then recalculated to a glass free basis.

Figure 9. Mineral chemistry (Ti-Fe-Mg-Mn) plots of biotite phenocrysts from the Vilama ignimbrite used for correlation with units previously mapped as different ignimbrites (data from Soler, 2005). Biotite compositions from the Atana and Sifón ignimbrites (Lindsay et al., 2001a, de Silva, 1989b) are plotted for comparison.

Figure 10. Major and trace elements plots showing the Vilama ignimbrite whole rock-compositions. Pumice and fiamme analyses are marked with arrows. The TAS classification diagram is according to Le Maitre (1989).

Figure 11. Diagrams showing the correlation between chemical composition and modal phenocryst variability in the Vilama ignimbrite. Elements that should be controlled by particular mineral phases (e.g. SiO_2-quartz, K_2O-biotite) show no correlation with variations in modal proportions of these phases. For each case, the correlation line was plotted, and

respective correlation coefficients (R) and slopes (S) are indicated. The generally low R and S values confirm that no correlation exists between crystal content and chemical composition variation in the Vilama ignimbrite. Symbols as in Fig. 10, without discriminating pumice and whole-rock data.

Figure 12. Interpreted model of collapse and resurgence of the Vilama caldera (the N-S profile schematically represents the cross section traced in Fig. 4).

A- Onset of the Vilama ignimbrite eruption. Caldera collapse starts, along with the emplacement of the outflow lower cooling unit (LCU) over an irregular paleotopography. Vents (central to fissure-like) are small as reflected by well-developed eruptive columns with efficient convective phases. The Vilama magma chamber is interpreted to be stretched out in NW-SE direction.

B- Complete development of faults that controlled the caldera floor subsidence. Large vents (mostly fissure-like) erupt enormous amounts of magma (~1800-1200 km^3) through low and sustained eruptive columns (boiling-over collapse fountains) that collapse mainly towards the downthrown side of inferred caldera faults. The outflow facies upper cooling unit (UCU), and the voluminous intracaldera fill, are deposited during this stage.

C- End of caldera collapse and eruption. The final geometry of the subsidence is uncertain and probably more complex than shown here.

D- Resurgence and post-caldera volcanism: doming of part of the intracaldera sequence and formation of a resurgent dome (RD); predominantly effusive post-collapse volcanism producing stratocones, domes and lavas (KS: Khastor stratovolcano; BD: Bayo dome; MNL: Mesada Negra lavas); erosion of the resurgent dome and infilling of caldera moat with sediments and post-caldera ignimbrites (LC: Laguna Coruto; LV: Laguna Vilama).

Table 1: Summary of characteristics of ignimbrite outcrops previously mapped as separate units, and now correlated with the redefined Vilama ignimbrite (VI). Whole-rock and mineral chemistry columns are comparisons of the composition of previous units with chemical features of the VI. Mineral abbreviations according to Kretz (1983).

Previously defined unit (Fig. 2)	Brief description	Sections described (Fig. 3)	Mineral assemblage	Age (Ma) (Table 3)	Stratigraphic relationship with outcrops originally ascribed to Vilama	Whole-rock and pumice chemistry (Fig. 10; Table 2)	Biotite chemistry (Fig. 9)	Correlation with the redefined Vilama ignimbrite (Fig. 5)
Outcrops previously ascribed to the Granada ignimbrite (Coira et al., 1996)	Gray-coloured, non- or weakly welded tuffs distributed over the same area as VI. The middle part may show moderate welding. Distal sections (8, 9) show minor fall and surge units.	1, 4, 8 and 9	bt+pl+qtz+ opx±hbl±cpx	8.2 ± 0.2	Always overlain by theVI. Upper contact with VI is sharp and erosive.	Similar	-	Extracaldera facies – LCU
Tobas Loromayu 1 (Almendras and Baldellón, 1996)	Non-welded to slightly welded tuffs W of Lag. Chojllas (Bolivia). Coarser facies than those described above. Lithic fragments up to 35 cm long.	26	bt+pl+qtz+ opx+hbl±cpx	8.6 ± 0.7 9.1 ± 0.5	No lateral or vertical relationship	Similar	Similar	Extracaldera facies - LCU
Ceja Grande ignimbite (Coira et al., 1996)	Intensely welded, black to reddish brown vitrophyric ignimbrite.	8, 9, and 10	bt+pl+qtz+ hbl+opx±cpx	8.3 ± 0.6	Underlaying the VI, to which it passes upwards gradually	Similar	Similar	Extracaldera facies - UCU
Capaderos ignimbrite (Coira et al., 1996)	Reddish to dark brown, welded ignimbrite with well developed subhorizontal jointing.	8, 9, and 10	bt+pl+qtz+ opx+cpx±hbl	-	Remarkable lateral continuity	Similar	-	Extracaldera facies - UCU
Tobas Lagunillas 1 (Pacheco and Ramírez, 1996)	Pink to purple-gray, moderately welded tuffs cropping out 20-40 km to the north from undisputed VI outcrops. Same field aspects as the VI in equivalent positions to the south	21 and 22	bt+pl+qtz+ opx±cpx±hbl	12.4 ± 0.4	No lateral relationship, but shows lateral continuity with Tobas Lagunillas 3 which closely matches the VI in position and lithology	Similar	Similar	Extracaldera facies - UCU
Tobas Lagunillas 2 (Pacheco and Ramírez, 1996)	Purple to dark brown, densely welded tuff with a tight subhorizontal jointing. It gradually passes upwards to Tobas La gunillas 3, being transitional both in welding grade and jointing.	19 and 20	bt+pl+qtz+ opx±cpx±hbl	9.3 ± 0.4	No direct relationship, but transitional pass to less welded Tobas Lagu nillas 3 suggests a welding profile similar to that observed to the south (Argentina) at sections 8, 9 and 10.	Similar	Similar	Extracaldera facies - UCU
Tobas Lagunillas 3 (Pacheco and Ramírez, 1996)	Welded ignimbrite with moderately well developed subhorizontal jointing.	14 to 18, and 23	bt+pl+qtz+ opx±cpx±hbl	9.0 ± 0.6 9.2 ± 0.3	No direct relationship, but occupying symmetrical positions respecting the inferred source area for VI	Similar	Similar	Extracaldera facies - UCU
Tobas Lupi Gera (Baker and Francis, 1978; Pacheco and Ramírez, 1996)	Welded ignimbrite with a well developed subhorizontal jointing.	24, 25	bt+pl+qtz+ opx+hbl (abundant hbl, scarce cpx)	7.9 ± 0.9	No direct relationship. It is partially separated from other outcrops correlated with VI by a barrier of older volcanic rocks.	Similar	-	Extracaldera facies - UCU (correlation tentative)
Toloma ignimbrite (Coira et al., 1996)	Thick tuff sequence comprised by multiple ignimbrite flow units with high induration and welding grade.	12	bt+pl+qtz+ cpx±opx±hbl	8.44 ± 0.4	It shows good continuity with updomed deposits located to the west (Tobas Coruto).	Similar	Similar	Intracaldera facies
Tobas Coruto (Almendras and Baldellón, 1996)	Thick tuff sequence comprising dark brown to purple ignimbrites with varying (usually high) induration and welding grade. The sequence forms an anticline.	13 and 27	bt+pl+qtz+ cpx±opx±hbl	8.46 ± 0.16 10.1 ± 0.1	No clear lateral continuity. Field resemblance with the VI, and updoming of rocks led Coi ra et al. (1996) to interpret a resurgent dome.	Similar	Similar	Intracaldera facies

Table 2: Representative chemical analyses of different facies of the Vilama ignimbrite

Facies	LCU	LCU	UCUb	UCUb	UCUt	UCUt	Intracaldera
Sample	M-186p[1]	M-203P[1]	M-217[2]	M-204[3]	M-194	M-216[4]	M-171
	pumice	pumice	tuff	tuff	tuff	tuff	tuff
SiO_2	63.90	63.51	66.34	67.62	63.42	63.80	62.81
TiO_2	0.88	0.90	0.80	0.51	0.96	0.91	0.76
Al_2O_3	15.93	16.64	15.59	14.09	17.10	16.82	16.46
Fe_2O_3t	5.05	4.83	4.37	3.05	5.41	5.04	4.40
MnO	0.05	0.06	0.05	0.04	0.06	0.06	0.04
MgO	1.74	1.72	1.52	1.26	1.80	1.75	1.68
CaO	3.83	4.28	3.77	2.69	4.60	4.65	4.18
Na_2O	2.25	2.12	2.30	2.43	2.28	2.13	2.47
K_2O	4.16	3.52	3.97	4.32	3.46	3.56	4.04
P_2O_5	0.19	0.19	0.17	0.11	0.18	0.18	0.18
LOI	0.97	2.03	0.65	2.45	0.94	0.97	1.06
Total	98.94	99.79	99.53	98.57	100.22	99.87	98.08
Y	20	21	19	17	18	18	20
Rb	169	155	166	188	126	141	163
Sr	239	289	243	205	282	268	259
Ba	634	709	548	541	672	630	626
U	4	3	4	10	3	3	5
Th	13	11	14	21	11	11	12
Zr	163	167	160	145	159	162	187
Nb	14	14	13	12	12	13	14
Cr	13	25	4	21	14	15	12
Ni	b.d.l	b.d.l.	b.d.l.	3	b.d.l	b.d.l	b.d.l
Co	38	25	24	21	19	49	18
Cu	4	b.d.l	2	8	b.d.l	4	b.d.l
Pb	17	20	58	35	21	19	20

Outflow facies: LCU and UCU are the lower and upper cooling units, subscripts t and b respectively referring to the base and top of the latter. b.d.l.: below detection level. All analyses obtained by XRF at the Instituto de Geología y Minería (Universidad Nacional de Jujuy, Argentina). Analytical procedures, sample preparation, and equipment characteristics as in Caffe et al. (2002).
[1]- ex- Granada ignimbrite; [2]- ex- Toba Lagunillas 2; [3]- ex- Ceja Grande ignimbrite; [4]- ex- Toba Lagunillas 3.

Table 3: Summary of published and new K/Ar and $^{40}Ar/^{39}Ar$ ages of units associated with the Vilama caldera

Stratigraphic unit		**Sample description**		**Age (Ma)**
Map location	**Reference**			
			(Fig. 4)	
Post-collapse units				
Bonanza ignimbrite	Bo-3; ignimbrite	6.2 ± 0.5 [a]	1	5
Loromayu stratovolcano	LB-43; lava	6.2 ± 0.5 [a]	2	6
Cerro Panizos ignimbrite	AMO-16; pumice	6.71 ± 0.04 [b]	3	10
Bayo dome	Y-50; lava*	7.49 ± 0.35 [a]	4	4
Khastor 2 dome	CP-10; lava	7.6 ± 0.6 [a]	5	9
Khastor 1 dome	CP-12; lava	7.6 ± 0.5 [a]	5	9
Cienago ignimbrite	AMO-22E; pumice	7.87 ± 0.59 [b]	6	10
Khastor 1 dome	QT-77; lava	8.1 ± 0.5 [a]	7	3
Salle ignimbrite	V-12; ignimbrite	8.4 ± 0.6 [a]	8	5
Syn-collapse units				
Vilama ignimbrite – intracaldera	M-171; ignimbrite	8.6 ± 0.9 [a]	9	1
		13.1 ± 0.3 [a]		1
Vilama ignimbrite – intracaldera	M-171; ignimbrite	5.4 ± 0.5 [b]	9	1
		33.5 ± 0.4 [b]		1
Vilama ignimbrite – intracaldera (ex – Toloma ignimbrite)	M-164p; pumice	8.44 ± 0.04 [b]	10	1
Vilama ignimbrite – intracaldera	M-233p; pumice	8.46 ± 0.16 [b]	11	1
Vilama ignimbrite – intracaldera (ex - Tobas Coruto)	LB-124; ignimbrite	10.2 ± 1.1 [a]	11	6
Vilama ignimbrite – UCUt	M-194; ignimbrite	8.53 ± 0.09 [b]	12	1
Vilama ignimbrite – UCUt	Y-48; ignimbrite	8.49 ± 0.25 [a]	13	4
Vilama ignimbrite – UCUt (ex - Tobas Lagunillas 3)	QT-48; ignimbrite	9.0 ± 0.6 [a]	14	3
Vilama ignimbrite – UCUt (ex - Tobas Lupi Gera)	ignimbrite	7.9 ± 0.9 [a]	15	7
Vilama ignimbrite – UCUt (ex - Tobas Lagunillas 1)	SO-47; ignimbrite	12.4 ± 0.4 [a]	16	8
Vilama ignimbrite – UCUt (ex - Tobas Lagunillas 3)	CP-47; ignimbrite	9.2 ± 0.3 [a]	17	9
Vilama ignimbrite – UCUb	M-51; ignimbrite	8.5 ± 0.3 [a]	18	1
Vilama ignimbrite – UCUb	M-204; ignimbrite	8.56 ± 0.15 [b]	19	1
Vilama ignimbrite – UCUb	M-205; ignimbrite	8.28 ± 0.13 [b]	19	1
Vilama ignimbrite – UCUb (ex - Ceja Grande ignimbrite)	Z-39; ignimbrite	8.3 ± 0.6 [a]	19	5
Vilama ignimbrite – UCUb (ex - Tobas Lagunillas 2)	QT-47; ignimbrite	9.3 ± 0.4 [a]	20	3
Vilama ignimbrite – LCU (ex - Granada ignimbrite)	M-258; ignimbrite	8.2 ± 0.2 [b]	18	1
Vilama ignimbrite – LCU (ex – Granada ignimbrite)	M-203p; pumice	8.8 ± 0.3 [b]	19	2
Vilama ignimbrite – LCU (ex - Tobas Loromayu 1)	LB-34; ignimbrite	8.6 ± 0.7 [a]	21	6
Vilama ignimbrite – LCU (ex - Tobas Loromayu 1)	LB-36; ignimbrite	9.1 ± 0.5 [a]	22	6
Pre-collapse units				
Granada ignimbrite	M-103p; pumice	9.7 ± 0.09 [b]	23	2
Ojo de Perico lavas	QT-33; lava	9.8 ± 0.7 [a]	24	3
Lagunillas ignimbrite	M-38p; pumice	10.25 ± 0.12 [b]	25	2

[a] K/Ar age; [b] $^{40}Ar/^{39}Ar$ age

All isotopic analyses performed on biotite, except in * (whole-rock)

References: 1) This work; 2) Caffe et al. (2006); 3) Pacheco and Ramírez (1996); 4) AQUATER (1979); 5) Coira et al. (2004); 6) Almendras and Baldellón (1996); 7) Baker and Francis (1978); 8) Pacheco and Ramírez (1997); 9) García (1997); 10) Ort (1993).

Table 4. Summary of analytical data of new $^{40}Ar/^{39}Ar$ dating (biotite) of the Vilama ignimbrite.

Section (Fig. 3)	Sample	Number of crystals or clusters analyzed	Number of crystals or clusters with irregular gas spectra	N° of steps forming plateaus (all selected crystals considered)	Age ± 2 σ (Ma)
4	M-258[a,1]	2	0	7	8.2 ± 0.2**
7	M-194[a]	3	3	0	8.53 ± 0.09***
8	M-204[a]	2	0	4	8.56 ± 0.15**
8	M-205[a]	2	0	6	8.28 ± 0.13**
12	M-164p[a]	2	0	9	8.44 ± 0.04*
13	M-171[a,1]	1	0	3	5.4 ± 0.5**
		1	1	0	33.5 ± 0.4****
27	M-233p[b,1]	2	1	4	8.46 ± 0.16**

[a] Whole-rock biotite; [b] Pumice biotite
*Isochron; **Average of plateau steps; *** Total fusion; ****Average of integrated ages
[1] Multiple crystal cluster, applied constant J= 5.5784E-03 ± 4.87E-06; for the remaining analyses, single crystal and J=3.5257E-03 ± 2.43E-06

Table 5. Analytical details of new K/Ar (whole-rock biotite) ages of the Vilama ignimbrite

Section (Fig. 3)	Sample	K (%)	^{40}Ar radiogenic (ppm)	^{40}Ar radiog / ^{40}Ar total	Age ± 2 σ (Ma)
4	M-51	7.453	0.004402	0.248	8.5 ± 0.3
13	M-171	7.349	0.004395	0.142	8.6 ± 0.9
		7.349	0.006722	0.209	13.1 ± 0.3

Applied constants: $\lambda_\theta + \lambda`_\theta = 0.581 \times 10^{-10}$ y.$^{-1}$; $\lambda_\beta = 4.962 \times 10^{-10}$ y.$^{-1}$; ^{40}K/K = 1.193×10^{-4}.g/g

Table 6. Summary of caldera parameters and calculated volumes (following Lipman, 1997) of the Vilama ignimbrite intracaldera deposits (tuff fill volume) assuming piston-like and trap-door-like geometries.

Caldera	Topo C diameter (D (km))	Structural diameter (d (km))	Subsidence depth (S (km))	Total collar height (H (km))	Collar slope, angle (A (angle))	Topo C area (Tca (km2))	Structure area (Sa (km2))	Structure volume (Sv(km3))	Collar area (Ca (km2))
	#	#	#	#	**	π (D/2)2	π (d/2)2	Sa * S	Tca - Sa
La Pacana	43.6	39.5	2.0	1.5	20	1493	1225	2451	268
Vilama 1	32	26.5	2.5	1.5	18	804	552	1379	253
Vilama 2			1.8	1.0				993	

Collar (lithic) volume (Cv (km3))	Topo C volume (full) (TCv (km3))	Collar percent (full) (C%)	Unfilled collar height (h (km))	Unfilled collar diameter (Cud (km))	Unfilled caldera volume (Cuv (km3))	Remaining caldera fill (Cf (km3))	Tuff fill volume (Tf (km3))	Caldera lithic fill (Cl (vol %))	Lithic-fill height, margin (Lh (km))
**	Sv + Cv	Cv / TCv * 100	#	**	**	TCv – Cuv	Cf – Cv	Cv / Cf * 100	3/2(Cv / Sa)
197	2648	7.4	0.50	42.2	723	1924	**1727**	10.2	0.24
245	1624	15.0	0.25	31.1	195	1429	**1184**	17.0	0.67
122	1115	11.0		30.6	193	922	**800**	13.0	0.33

Vilama 1 and 2: piston-like and trap-door collapse, respectively. For Vilama 2 only parameters which differ from Vilama 1 are shown. Calculations for the La Pacana caldera are shown for comparison (data from Lindsay et al., 2001a).

# indicates observed or estimated dimension (see Lipman, 1997; Figure 1). ** additional formulae: $A = \tan^{-1} H/((D-d)/2)$; $Cv = \pi H(D^3-3D*d^2+2d^3)/12(D-d)$; $Cud = d+(D-d)*(H-h)/H$; $Cuv = \pi h/12[(D^3-Cud^3)/D-Cud)]$. “Topo C” refers to topographic caldera; “Collar” refers to the collapsed area produced by mass wasting, and scarp retreat. Vilama caldera diameters refer to caldera equivalent circles (Topo C is equivalent to the area enclosed by a topographic rim of 20 x 40 km, assuming an average distance of ~5 km between topographic and structural rims. Structural diameter is equivalent to the area enclosed within the caldera structural border). The total collar height for the Vilama caldera was estimated from values proposed by Lipman (1997) and Lindsay et al. (2001a) for other calderas of similar size.

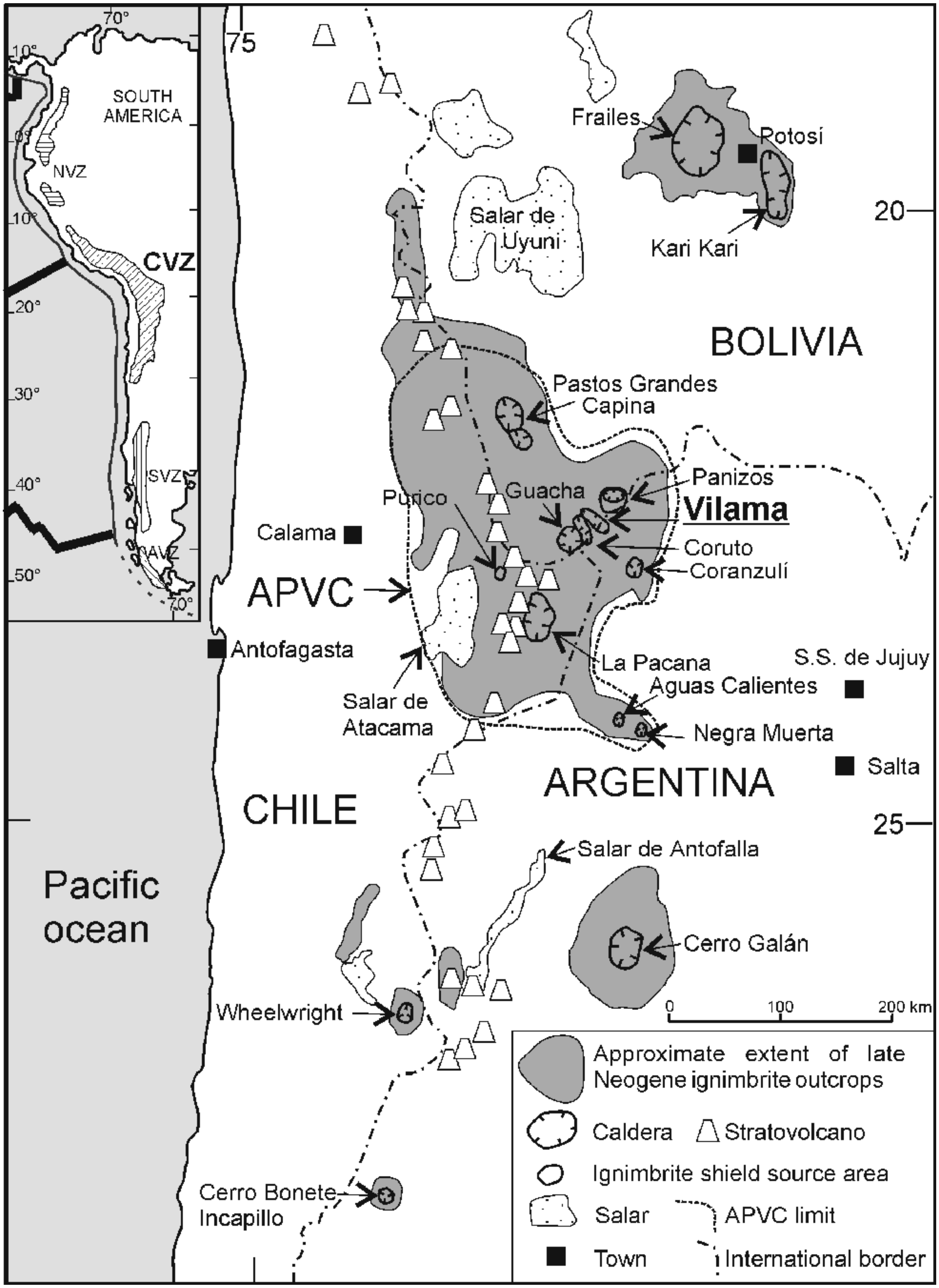

70°
10°
SOUTH AMERICA
0°
NVZ
10°
CVZ
20°
30°
SVZ
40°
AVZ
50°
70°
75
20
25
Frailes
Potosí
Kari Kari
Salar de Uyuni
BOLIVIA
Pastos Grandes
Capina
Panizos
Guacha
Vilama
Purico
Coruto
Coranzulí
Calama
APVC
Antofagasta
La Pacana
Aguas Calientes
S.S. de Jujuy
Salar de Atacama
Negra Muerta
Salta
ARGENTINA
CHILE
Salar de Antofalla
Pacific ocean
Cerro Galán
Wheelwright
0
100
200 km
Approximate extent of late Neogene ignimbrite outcrops
Caldera
Stratovolcano
Ignimbrite shield source area
Salar
APVC limit
Town
International border
Cerro Bonete Incapillo

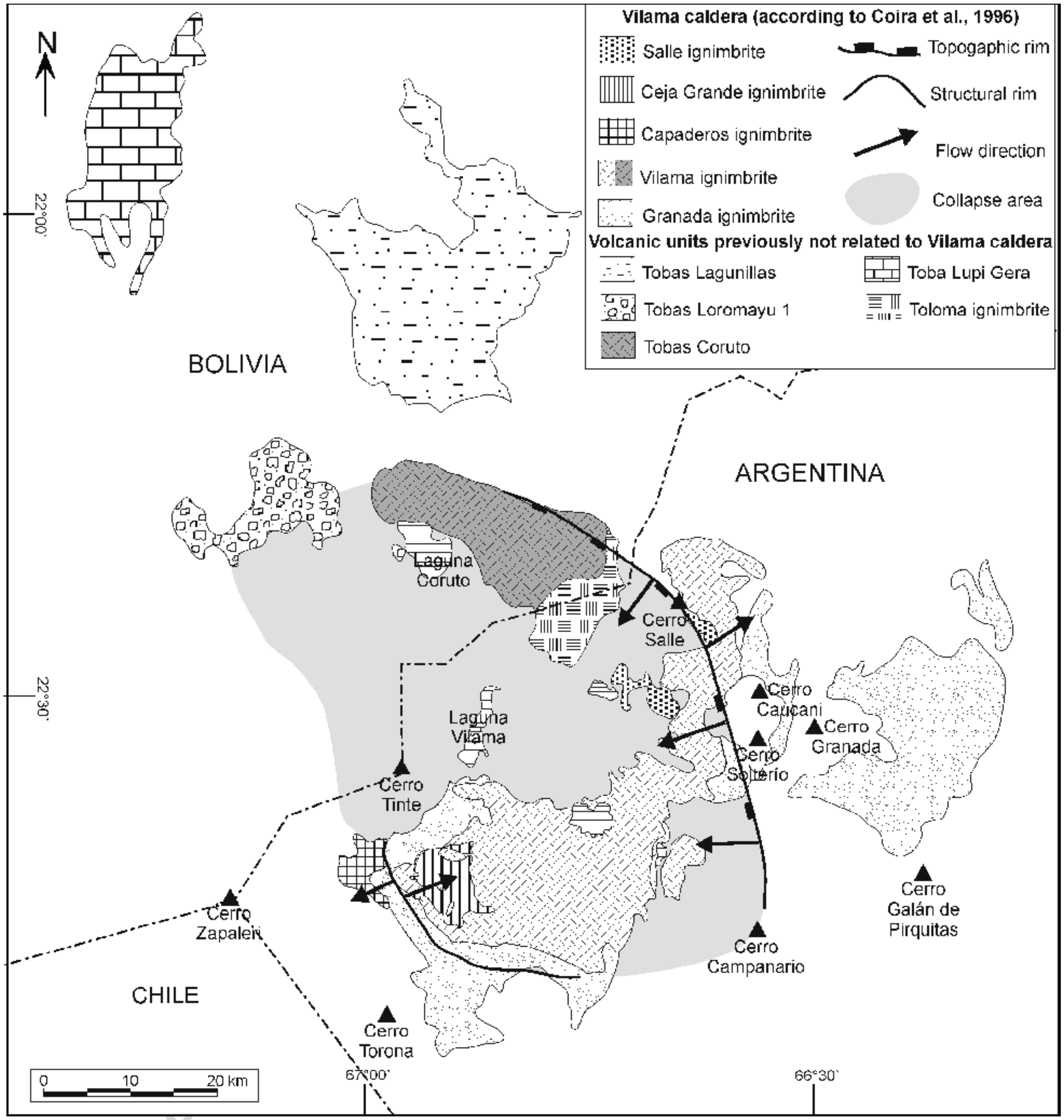

Vilama caldera (according to Coira et al., 1996)
Salle ignimbrite
Ceja Grande ignimbrite
Capaderos ignimbrite
Vilama ignimbrite
Granada ignimbrite
Topogaphic rim
Structural rim
Flow direction
Collapse area
Volcanic units previously not related to Vilama caldera
Tobas Lagunillas
Tobas Loromayu 1
Tobas Coruto
Toba Lupi Gera
Toloma ignimbrite
N
22°00'
22°30'
BOLIVIA
ARGENTINA
CHILE
Laguna Coruto
Laguna Vilama
Cerro Salle
Cerro Caucani
Cerro Granada
Cerro Solterío
Cerro Tinte
Cerro Zapaleri
Cerro Campanario
Cerro Galán de Pirquitas
Cerro Torona
0
10
20 km
67°00'
66°30'

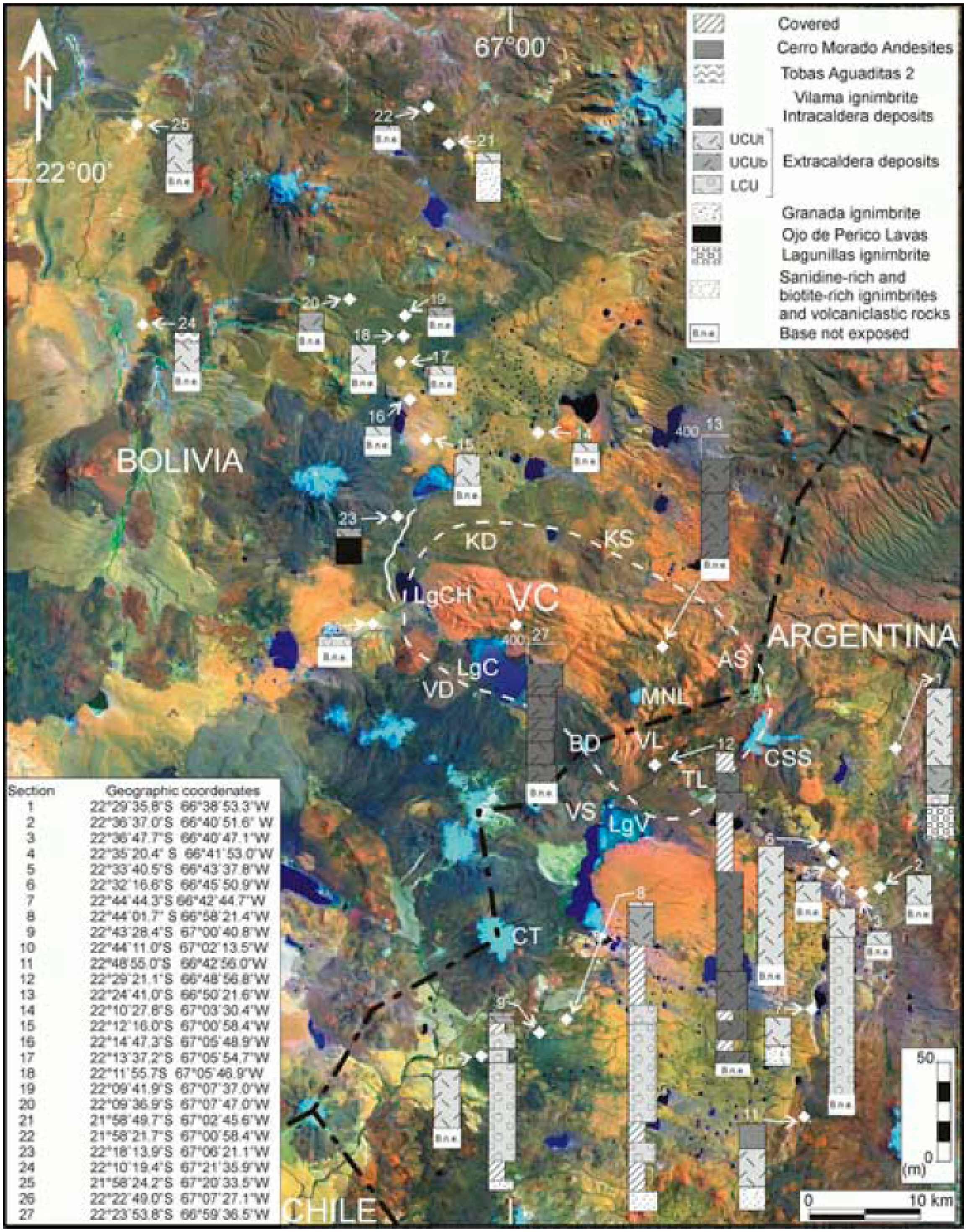
67°00'
22°00'
N
Covered
Cerro Morado Andesites
Tobas Aguaditas 2
Vilama ignimbrite
Intracaldera deposits
UCUt
UCUb
LCU
Extracaldera deposits
Granada ignimbrite
Ojo de Perico Lavas
Lagunillas ignimbrite
Sanidine-rich and biotite-rich ignimbrites and volcaniclastic rocks
B.n.e
Base not exposed
BOLIVIA
ARGENTINA
CHILE
VC
KD
KS
LgCH
LgC
VD
AS
MNL
BD
VL
TL
CSS
VS
LgV
CT
400
50
0
(m)
0
10 km
Section
Geographic coordenates
1 22°29'35.8"S 66°38'53.3"W
2 22°36'37.0"S 66°40'51.6" W
3 22°36'47.7"S 66°40'47.1"W
4 22°35'20.4" S 66°41'53.0"W
5 22°33'40.5"S 66°43'37.8"W
6 22°32'16.6"S 66°45'50.9"W
7 22°44'44.3"S 66°42'44.7"W
8 22°44'01.7" S 66°58'21.4"W
9 22°43'28.4"S 67°00'40.8"W
10 22°44'11.0"S 67°02'13.5"W
11 22°48'55.0"S 66°42'56.0"W
12 22°29'21.1"S 66°48'56.8"W
13 22°24'41.0"S 66°50'21.6"W
14 22°10'27.8"S 67°03'30.4"W
15 22°12'16.0"S 67°00'58.4"W
16 22°14'47.3"S 67°05'48.9"W
17 22°13'37.2"S 67°05'54.7"W
18 22°11'55.7S 67°05'46.9"W
19 22°09'41.9"S 67°07'37.0"W
20 22°09'36.9"S 67°07'47.0"W
21 21°58'49.7"S 67°02'45.6"W
22 21°58'21.7"S 67°00'58.4"W
23 22°18'13.9"S 67°06'21.1"W
24 22°10'19.4"S 67°21'35.9"W
25 21°58'24.2"S 67°20'33.5"W
26 22°22'49.0"S 67°07'27.1"W
27 22°23'53.8"S 66°59'36.5"W

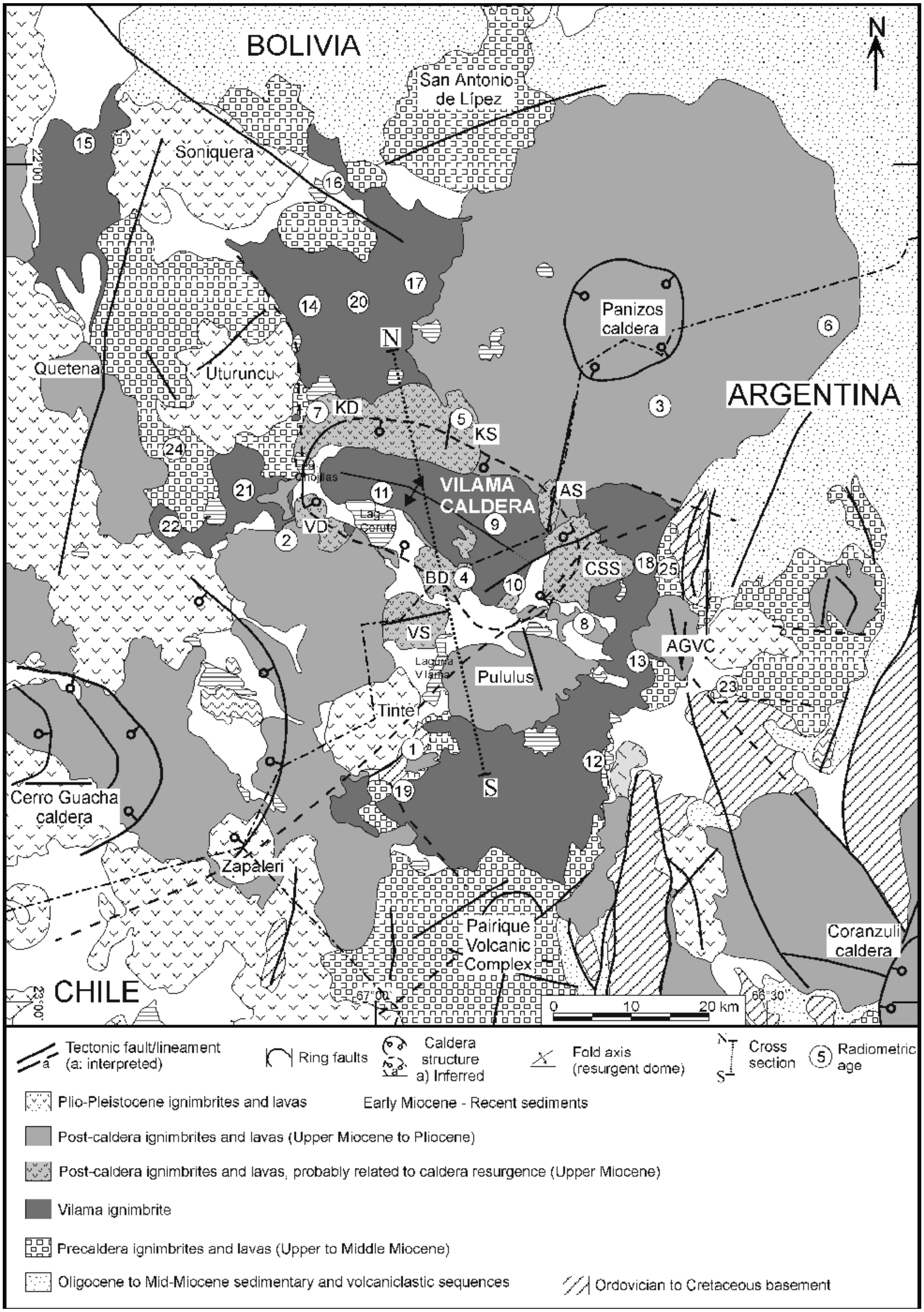
BOLIVIA
N
San Antonio de Lípez
Soniquera
15
16
22°00'
17
14
20
Panizos caldera
6
Quetena
Uturuncu
ARGENTINA
3
7
KD
5
KS
24
Lag. Chojllas
21
11
VILAMA CALDERA
AS
22
2
VD
Lag. Coruto
9
18
25
CSS
BD
4
10
8
VS
AGVC
Laguna Vilama
Pululus
13
23
Tinte
1
12
19
S
Cerro Guacha caldera
Zapaleri
Pairique Volcanic Complex
Coranzuli caldera
CHILE
23°00'
67°00'
66°30'
0
10
20 km
Tectonic fault/lineament
a
(a: interpreted)
Ring faults
Caldera structure
a) Inferred
Fold axis (resurgent dome)
N
S
Cross section
5
Radiometric age
Plio-Pleistocene ignimbrites and lavas
Early Miocene - Recent sediments
Post-caldera ignimbrites and lavas (Upper Miocene to Pliocene)
Post-caldera ignimbrites and lavas, probably related to caldera resurgence (Upper Miocene)
Vilama ignimbrite
Precaldera ignimbrites and lavas (Upper to Middle Miocene)
Oligocene to Mid-Miocene sedimentary and volcaniclastic sequences
Ordovician to Cretaceous basement

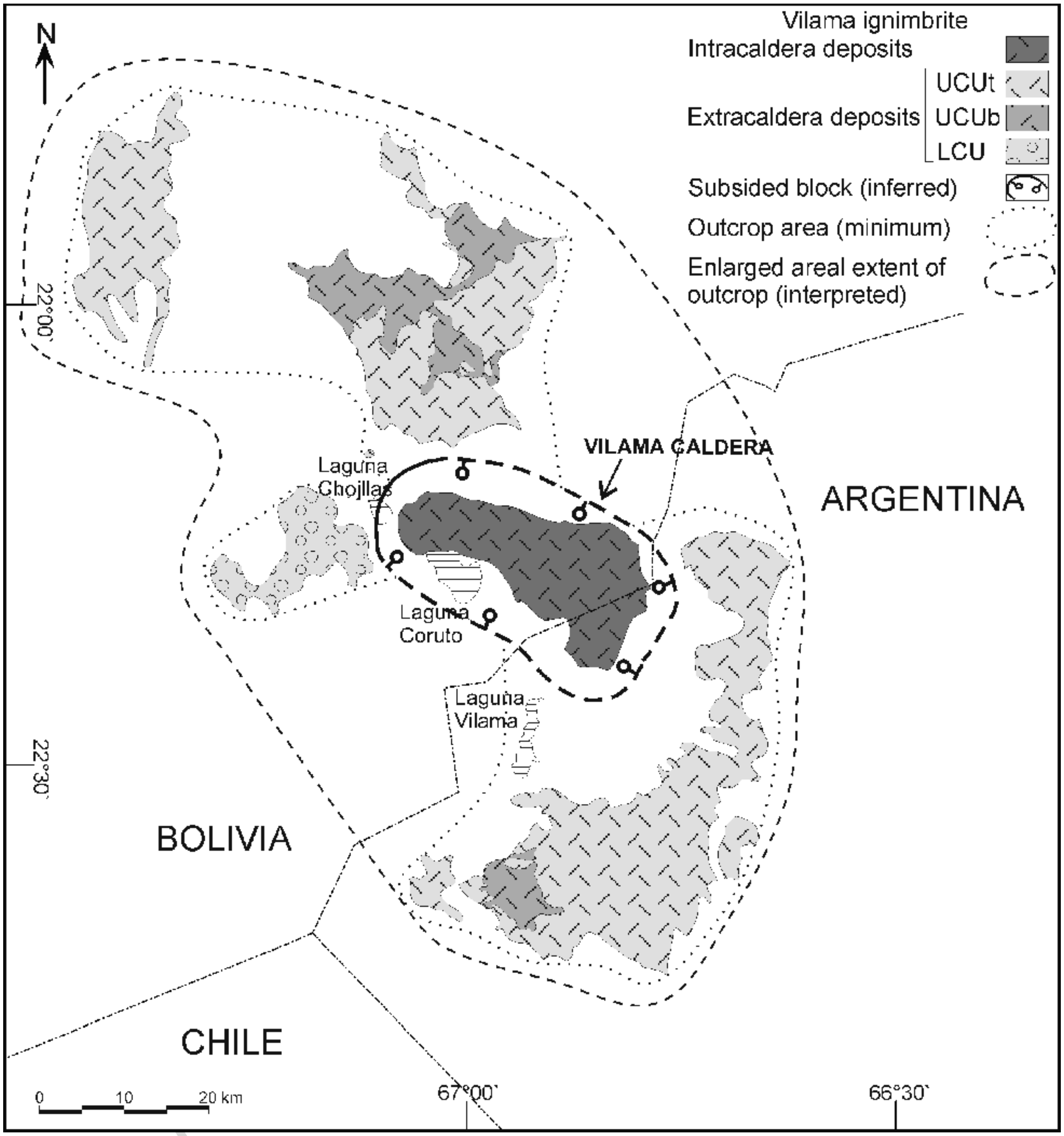

N
Vilama ignimbrite
Intracaldera deposits
Extracaldera deposits
UCUt
UCUb
LCU
Subsided block (inferred)
Outcrop area (minimum)
Enlarged areal extent of
outcrop (interpreted)
22°00'
22°30'
VILAMA CALDERA
Laguna
Chojllas
Laguna
Coruto
Laguna
Vilama
ARGENTINA
BOLIVIA
CHILE
0
10
20 km
67°00'
66°30'

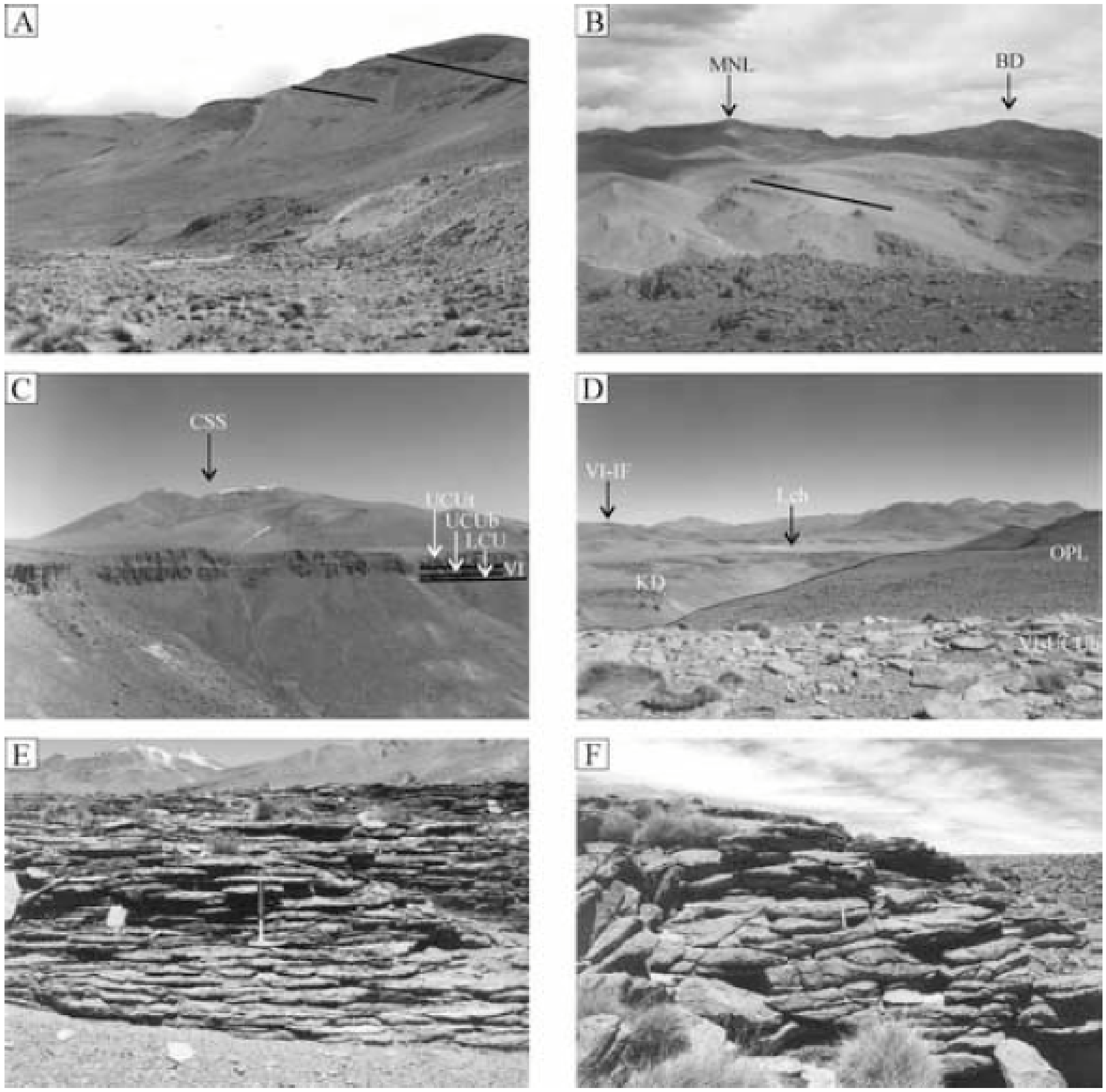
A
B
MNL
BD
C
CSS
UCUt
UCUb
LCU
VI
D
VI-IF
Lch
KD
OPL
E
F

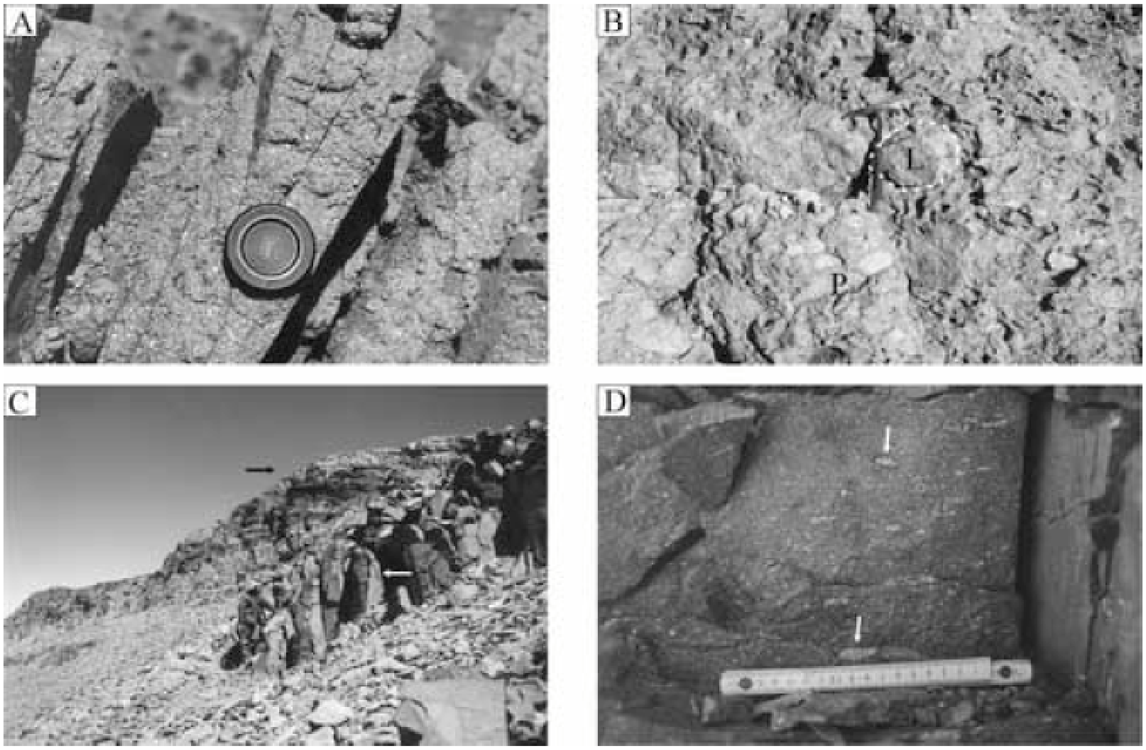
A
B
L
P
C
D

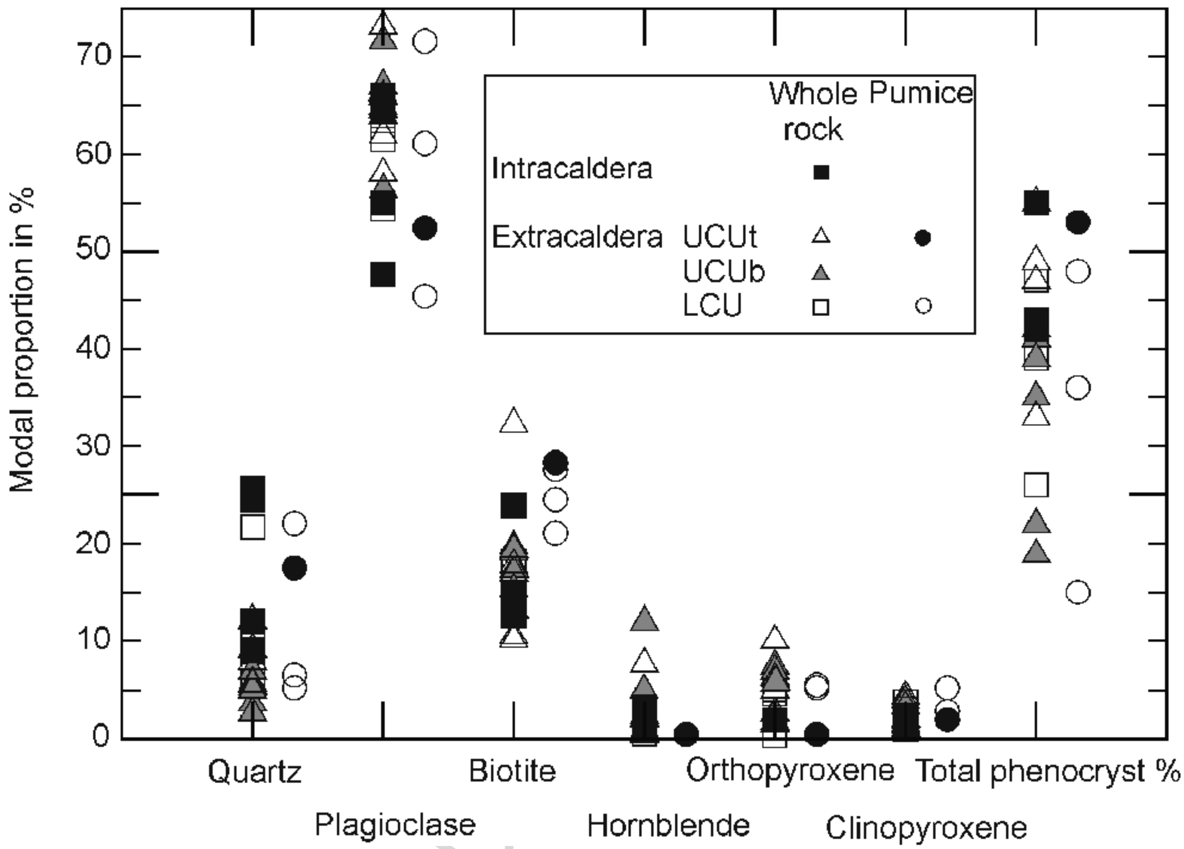

Modal proportion in %
0
10
20
30
40
50
60
70
Whole rock
Pumice
Intracaldera
Extracaldera
UCUt
UCUb
LCU
Quartz
Plagioclase
Biotite
Hornblende
Orthopyroxene
Clinopyroxene
Total phenocryst %

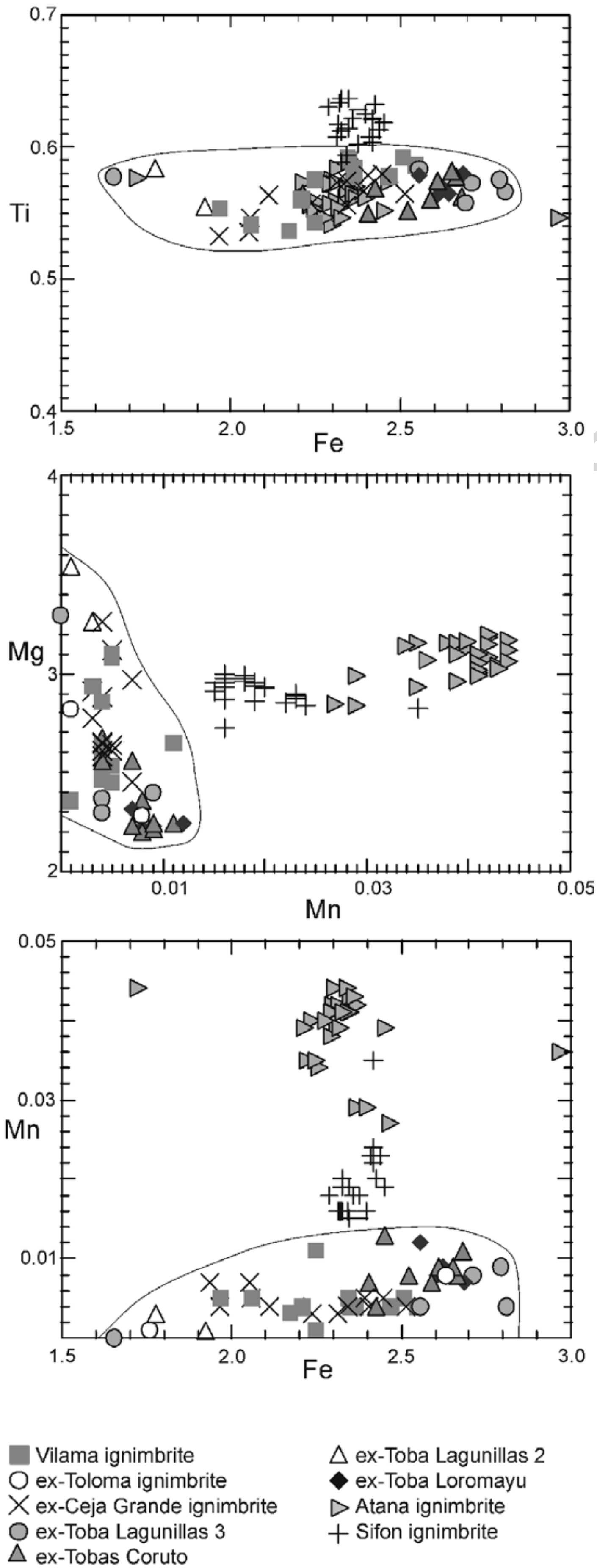
0.7
0.6
0.5
0.4
Ti
1.5
2.0
2.5
3.0
Fe
4
3
2
Mg
0.01
0.03
0.05
Mn
0.05
0.03
0.01
Mn
1.5
2.0
2.5
3.0
Fe
Vilama ignimbrite
ex-Toloma ignimbrite
ex-Ceja Grande ignimbrite
ex-Toba Lagunillas 3
ex-Tobas Coruto
ex-Toba Lagunillas 2
ex-Toba Loromayu
Atana ignimbrite
Sifon ignimbrite

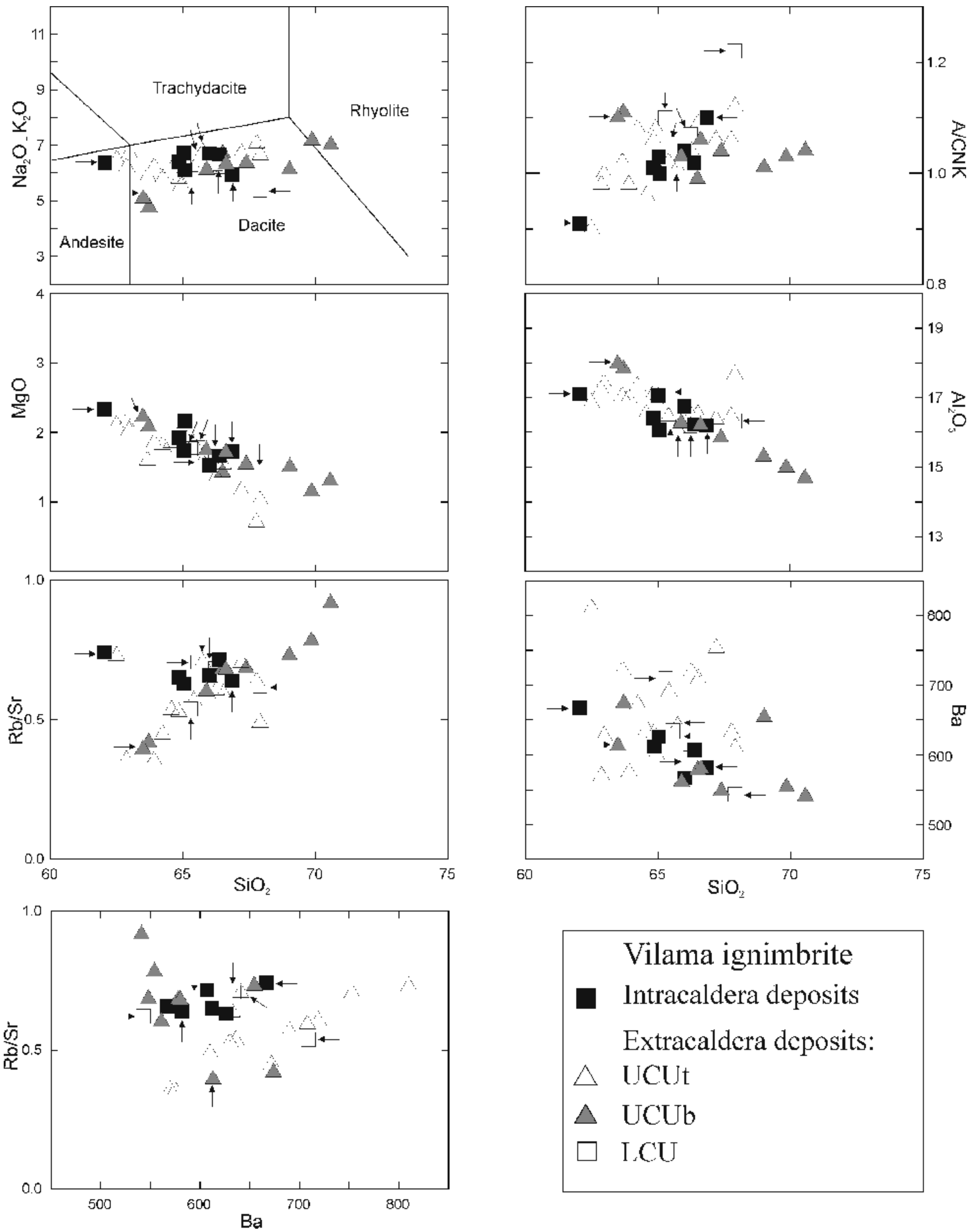

Trachydacite
Rhyolite
Andesite
Dacite
Na2O_K2O
A/CNK
MgO
Al2O3
Rb/Sr
Ba
SiO2
Vilama ignimbrite
Intracaldera deposits
Extracaldera deposits:
UCUt
UCUb
LCU

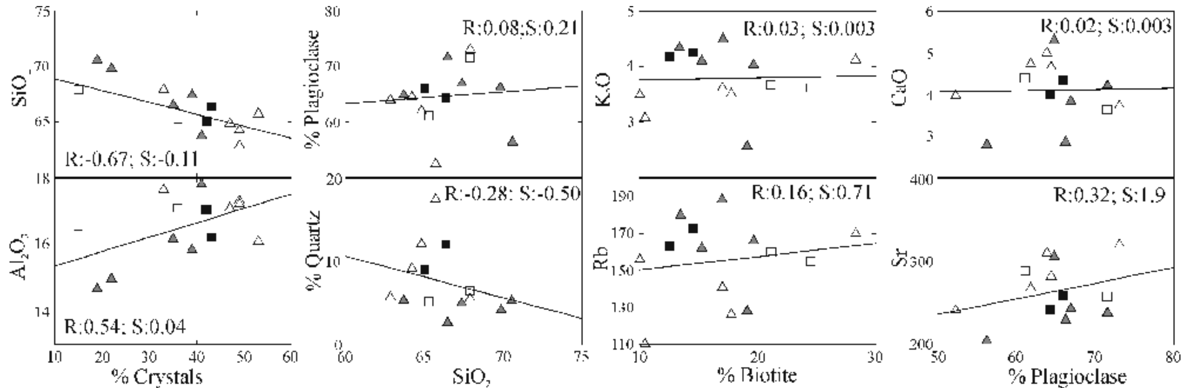
R:-0.67; S:-0.11
R:0.54; S:0.04
R:0.08;S:0.21
R:-0.28; S:-0.50
R:0.03; S:0.003
R:0.16; S:0.71
R:0.02; S:0.003
R:0.32; S:1.9
% Crystals
SiO_2
% Biotite
% Plagioclase
% Quartz
Al_2O_3
K_2O
CaO
Rb
Sr

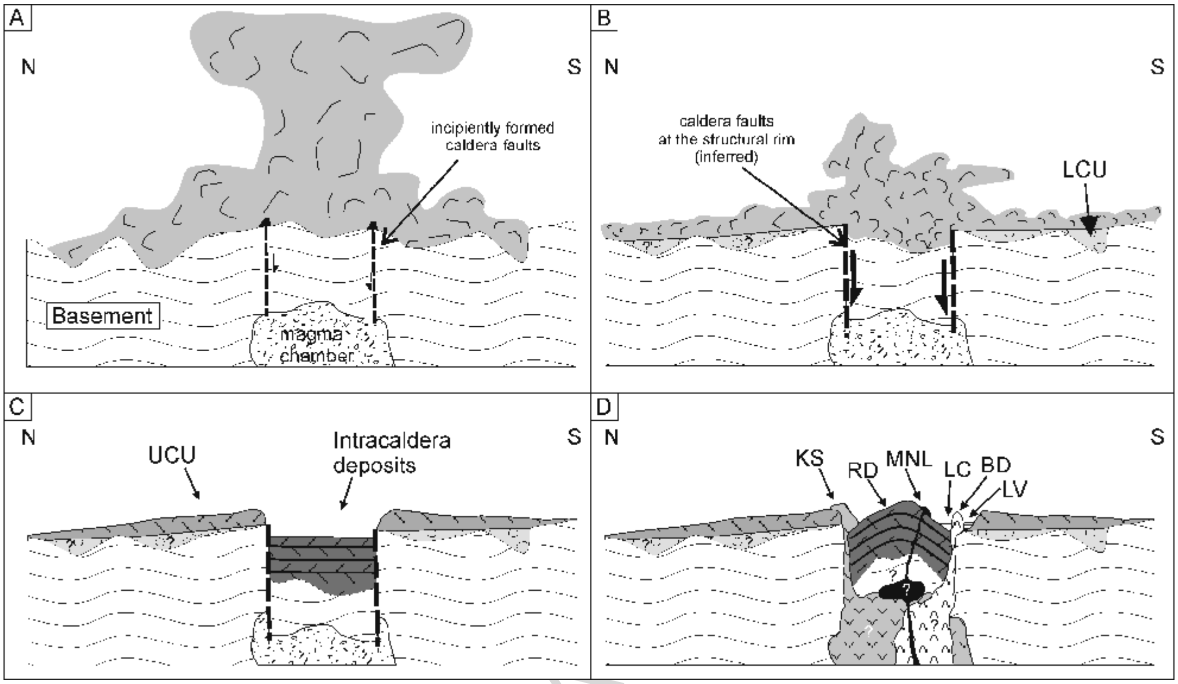
A
N
S
incipiently formed
caldera faults
Basement
magma
chamber
B
caldera faults
at the structural rim
(inferred)
LCU
C
UCU
Intracaldera
deposits
D
KS
RD
MNL
LC
BD
LV